

ABSTRACT

Title of Dissertation: **Estimation of Land Surface Radiation Budget from MODIS Data**

Hye-Yun Kim, Doctor of Philosophy, 2008

Directed By: Dr. Shunlin Liang, Professor
Department of Geography

Land Surface Radiation Budget (SRB) is responsible for the available energy between the Earth and atmosphere system. Net radiation is the driving force for the transportation and exchange of all matter at the interface between the Earth's surface and the atmosphere, and therefore, significantly affects the climatic forming and change. Accurate estimation of shortwave net radiation (S_n), cloudy-sky allwave net radiation (R_n), and daily integrated S_n at high spatial resolution is essential in regional and global land surface models.

The current SRB products have fine temporal and coarse spatial resolutions not suitable for land applications. New hybrid algorithm for S_n estimation has been developed in this study. S_n is estimated from MODIS data under both clear- and cloudy-sky conditions without requiring coarser resolution ancillary data. Therefore, estimated S_n retains the spatial resolution of the raw input data.

Surface all-wave (both shortwave and longwave) net radiation (R_n) controls the input of latent and sensible heat flux into the atmosphere over the Earth's surface.

Meteorological datasets are spatially limited and satellite data have the advantage of global spatial coverage; however, difficulty in accurately estimating cloudy-sky longwave net radiation (L_n) undermines efforts to estimate cloudy-sky all-wave net radiation. This study presents methods for estimating cloudy-sky R_n using S_n and other surface variables at 1 km spatial resolution.

Daily integrated S_n is closely related to carbon, water and energy flux simulations. A daily integrated S_n product with a 1-km spatial resolution supports recent high resolution numerical climate and ecosystem simulations. This study describes a method for estimating daily integrated S_n in 1 km resolution based on instantaneous S_n data.

All these algorithms have been validated using seven sites of a SURFace RADiation budget observing network (SURFRAD) in United States, instantaneous S_n is also compared with GEWEX/SRB and ISCCP data.

The new hybrid algorithm developed in the study can be easily implemented to generate operational global products. These finer spatial resolution datasets capture the specific sequence of the redistribution of the available energy at the Earth's surface; therefore, they support recent high resolution land surface models.

**Estimation of Land Surface Radiation Budget
from MODIS Data**

By

Hye-Yun Kim

Dissertation submitted to the Faculty of the Graduate School of the
University of Maryland, College Park, in partial fulfillment
of the requirements for the degree of
Doctor of Philosophy
2008

Advisory Committee:
Dr. Shunlin Liang, Chair
Dr. Ivan Csizsar
Dr. Zhanqing Li
Dr. John Townshend
Dr. In-Young Yeo

© Copyright by
Hye-Yun Kim
2008

Dedication

To my parents and family

Acknowledgements

I am deeply indebted to my advisor, Dr. Shunlin Liang whose logistical supports, stimulating discussion, helpful suggestions, and encouragement, as well as funding assisted me from my entrance to the graduate program at the University of Maryland through the research and writing stage of this dissertation. I also would like to thank the other members of my doctoral committee: Dr. Ivan Csiszar, Dr. Zhanqing Li, Dr. John Townshend, and Dr. In-Young Yeo. They provided valuable suggestions and recommendations for my research. I am also grateful to my previous advisors, Dr. Alexander F.H. Goetz and Dr. Joong-Sun Won, for broadening my vision of academic fields.

My heartfelt appreciation also goes to my parents and family for their valuable support of my academic pursuit. Despite the distance that separates us, you are always in my heart.

I would like to express my gratitude to all those who provided research assistance: Dr. Hongliang Fang, Dr. Tao Zheng, Dr. Wenhui Wang, and PhD candidate Mr. Dongdong Wang. I appreciate and value the discussions and suggestions from Dr. Kaicun Wang, research associate in the Department of Geography. I would also like to extend my gratitude to Dr. Alex Ritter for proofreading the draft of this dissertation.

Table of Contents

Dedication.....	ii
Acknowledgements.....	iii
Table of Contents.....	iv
List of Tables.....	vi
List of Figures.....	vii
Chapter 1: Introduction.....	1
1.1 Background.....	1
1.2 Need for surface net radiation with high spatial resolution.....	3
1.3 Objectives of this study.....	9
Chapter 2: Estimating Shortwave Net Radiation Using MODIS Data.....	12
2.1 Existing methods for surface shortwave net radiation estimates.....	15
2.2 Theoretical basis of the new hybrid algorithm.....	18
2.2.1 Radiative transfer simulation.....	20
2.2.2 Linking TOA reflectance and shortwave net radiation.....	21
2.2.3 Water vapor correction.....	23
2.2.4 Elevation correction.....	26
2.3 Data sets.....	27
2.3.1 Surface reflectance spectra.....	28
2.3.2 MODIS products.....	28
2.3.2 Surface measurements.....	29
2.4 Validation.....	31
2.4.1 Hybrid algorithm: Direct estimation.....	32
2.4.2 Hybrid algorithm: Albedo-based estimation.....	36
2.4.3 Data aggregation using direct estimation.....	39
2.5 Comparison with other products.....	42
2.5.1 Comparison with GEWEX data.....	42
2.5.2 Comparison with ISCCP data.....	44
2.5.3 Comparison with a physically based method.....	46
2.6 Summary.....	48
Chapter 3: Estimating Cloudy-sky Net Radiation.....	52
3.1 Background.....	52
3.2 Cloudy-sky net radiation estimation method.....	54
3.2.1 Identifying cloudy-sky conditions.....	55
3.2.2 Multivariate regression analysis.....	57
3.2 Validation results.....	59
Chapter 4: Daily Net Radiation Estimation.....	62
4.1 Estimation algorithm.....	63
4.2 Validation.....	66
Chapter 5: Conclusions and future research.....	69
5.1 Estimating shortwave net radiation using MODIS data.....	69
5.2 Estimating cloudy-sky all-wave net radiation.....	70
5.3 Estimating daily integrated shortwave net radiation using MODIS data.....	70

5.4 Future research issues	72
Acronyms	76
Bibliography	77

List of Tables

TABLE 1- 1 SUMMARY OF SRB PRODUCTS.....	2
TABLE 1- 2 MODIS SPECTRAL BAND SPECIFICATION.....	7
TABLE 2- 1 COMPARISON OF WATER VAPOR TRANSMISSION CALCULATION.....	25
TABLE 2- 2 LOCATION OF SURFRAD SITES	30
TABLE 2- 3. VALIDATION OF ESTIMATED SHORTWAVE NET RADIATION USING HYBRID METHOD (DIRECT ESTIMATION) AT 1-KM AND TIME CLOSEST TO SATELLITE OVERPASS	33
TABLE 2- 4 VALIDATION OF ESTIMATED SHORTWAVE NET RADIATION USING HYBRID METHOD (ALBEDO-BASED ESTIMATION) AT 1 KM AND TIME CLOSEST TO SATELLITE OVER PASS.....	38
TABLE 2- 5 VALIDATION OF ESTIMATED SHORTWAVE NET RADIATION USING HYBRID METHOD (DIRECT ESTIMATION) AT 9 KM AND 30 MINUTE TIME WINDOW	40
TABLE 2- 6 COMPARISON OF SHORTWAVE NET RADIATION FROM GEWEX/SRB DATA (1 DEGREE RESOLUTION) FROM JANUARY TO JUNE 2005 FOR THE SEVEN SURFRAD SITES	44
TABLE 2- 7 COMPARISON OF SHORTWAVE NET RADIATION FROM ISCCP DATA (2.5 DEGREE RESOLUTION) 2004 FOR THE SEVEN SURFRAD SITES	44
TABLE 2- 8 SHORTWAVE NET RADIATION ESTIMATION VALIDATION FOR THE SEVEN SURFRAD SITES USING THE PHYSICALLY-BASED METHOD.....	46
TABLE 2- 9 COMPARISONS OF HYBRID METHOD (1 KM), GEWEX/SRB (1 DEGREE), AND ISCCP DATA (2.5 DEGREE). RMSE AS A PERCENTAGE OF MEAN OBSERVATION IS PRESENTED IN PARENTHESIS. RMSE AND BIAS ARE IN UNIT OF Wm^{-2}	50
TABLE 3- 1 LOCATION AND PLANT FUNCTIONAL TYPES (PFT) OF FLUXNET SITES USED IN SURFACE ALL-WAVE NET RADIATION STUDY	55
TABLE 3- 2 REGRESSION COEFFICIENTS USED TO ESTIMATE CLOUDY-SKY ALL-WAVE NET RADIATION	58
TABLE 3- 3 ERRORS RELATED TO SURFACE RADIATION BUDGET COMPONENTS ESTIMATION UNDER CLOUDY-SKY: (A) BONDVILLE, IL AND (B) PENN STATE, PA	61
TABLE 4- 1 VALIDATION OF DAILY INTEGRATED SHORTWAVE NET RADIATION, IN JOULES PER SQUARE METER, AT SEVEN SURFRAD SITES.....	66

List of Figures

FIGURE 2- 1 FLOWCHART DEPICTING THE HYBRID ALGORITHM FOR SHORTWAVE NET RADIATION ESTIMATION. ABOVE THE DASHED RED LINE INDICATES PHYSICAL PART OF THE HYBRID ALGORITHM AND BELOW INDICATES STATISTICAL PART OF THE HYBRID ALGORITHM.....	19
FIGURE 2- 2 SCHEME SHOWING THE RELATIONSHIP BETWEEN VARIABLE, HIDDEN NEURONS (HN), OUTPUT NEURONS (ON), AND PREDICTED OUTPUTS (Y_p) (ADAPTED FROM NOBLE AND TRIBOU, 2007).....	23
FIGURE 2- 3 ANN WORKING SCHEME.....	23
FIGURE 2- 4 NORMALIZED ELEVATION COEFFICIENTS DEPENDING ON SOLAR ZENITH ANGLE.....	27
FIGURE 2- 5 SEVEN SURFRAD SITES.....	30
FIGURE 2- 6 SIMULATED SHORTWAVE NET RADIATION FITTING USING MULTIVARIATE LINEAR REGRESSION (TOP) AND ARTIFICIAL NEURAL NETWORK (BOTTOM).....	34
FIGURE 2- 7 VALIDATION OF SHORTWAVE NET RADIATION ESTIMATION USING HYBRID METHOD (DIRECT ESTIMATION) FOR THE SURFRAD SITES.....	35
FIGURE 2- 8 VALIDATION OF SHORTWAVE NET RADIATION ESTIMATION USING HYBRID METHOD (ALBEDO-BASED ESTIMATION) FOR SURFRAD SITES.....	37
FIGURE 2- 9 SHORTWAVE NET RADIATION ESTIMATION USING ALBEDO-BASED ESTIMATION OVER PSU SITES. TOP: ALBEDO VALUES USED IN ALBEDO-BASED SHORTWAVE NET RADIATION ESTIMATION, MIDDLE: ESTIMATED SHORTWAVE DOWNWARD RADIATION, AND BOTTOM: ESTIMATED SHORTWAVE NET RADIATION USING ALBEDO-BASED ESTIMATION.....	39
FIGURE 2- 10 VALIDATION OF ESTIMATED SHORTWAVE NET RADIATION USING HYBRID METHOD (DIRECT ESTIMATION) AT 9 KM AND 30 MINUTE TIME WINDOW.....	41
FIGURE 2- 11 COMPARISON OF SHORTWAVE NET RADIATION FROM GEWEX/SRB DATA FROM JANUARY TO JUNE 2005 FOR THE SURFRAD SITES.....	43
FIGURE 2- 12 COMPARISON OF SHORTWAVE NET RADIATION FROM ISCCP DATA (2.5 DEGREE RESOLUTION) 2004 FOR THE SURFRAD SITES.....	45
FIGURE 2- 13 VALIDATION RESULTS FOR PHYSICALLY-BASED METHOD FOR SHORTWAVE NET RADIATION ESTIMATION.....	47
FIGURE 2- 14 COLOR COMPOSITE OF MODIS TOA REFLECTANCE OVER SOUTHERN LAKE MICHIGAN, ACQUIRED ON DAY 99 IN 2005 AND ESTIMATED SHORTWAVE NET RADIATION BY DIRECT ESTIMATION. UNITS ARE IN Wm^{-2}	51
FIGURE 3- 1 VARIATION IN CLEAR-SKY SHORTWAVE DOWNWARD RADIATION OVER THE COURSE OF ONE DAY.....	56
FIGURE 3- 2 FIELD CLOUDY-SKY ALL-WAVE NET RADIATION AND SHORTWAVE NET RADIATION.....	57
FIGURE 3- 3 CLOUDY-SKY ALL-WAVE NET RADIATION FITTING DEPENDANT ON PLANT FUNCTIONAL TYPES.....	59
FIGURE 3- 4 VALIDATION OF ALL-WAVE NET RADIATION ESTIMATION UNDER CLOUDY-SKY FOR BROADLEAF CROP PLANT FUNCTIONAL TYPE.....	60

FIGURE 4- 1 VARIATION IN GROUND MEASUREMENTS OF PHOTOSYNTHETICALLY ACTIVE RADIATION (PAR) AND SHORTWAVE NET RADIATION (S_N) IN FORT PECK, MT OVER THE COURSE OF FIVE DAYS	64
FIGURE 4- 2 VALIDATION OF DAILY INTEGRATED SHORTWAVE NET RADIATION AT SEVEN SURFRAD SITES	67

Chapter 1: Introduction

The Surface Radiation Budget (SRB) is a key factor responsible for the redistribution of the available energy in the Earth-atmosphere system. The spatial and temporal variation of SRB can be estimated from the satellite data because the solar radiation at the Earth's surface is strongly correlated to solar radiation reflected to space.

1.1 Background

Most land surface models rely on incoming radiation, such as those in the Global Energy and Water cycle EXperiment (GEWEX) (Pinker et al., 1995; Pinker et al., 2003), Community Climate System Model (CCSM) (Collins et al., 2006), and NOAA land surface model (LSM) (De Haan and Kanamitsu, 2007). The SRB is also required by short-term numerical weather prediction models and longer-term simulations for climate prediction.

Two major satellite-derived SRB products are available. One is derived from the International Satellite Cloud Climatology project (ISCCP) C1 data (Pinker and Laszlo, 1992) and the Earth Radiation Budget Experiment (ERBE) data. ISCCP-FD data have been used to estimate global monthly mean Surface Radiation Budget (SRB) (Zhang et al., 2004). The other product is derived from the Clouds and the Earth's Radiant Energy System (CERES), on board of the National Aeronautics and

Space Administration (NASA) Earth Observing System (EOS) satellites and the Tropical Rainfall Measuring Mission (TRMM) satellite (Wielicki et al., 1998). Current SRB products that are downloadable from websites and that provide an assessment of their accuracy are summarized in Table 1-1. I did not include products that lack an assessment of their accuracy (e.g. GEWEX Continental scale International Project and GEWEX Americas Prediction Project (GCIP/GAPP) surface radiation budget data).

Table 1- 1 Summary of SRN products

Products	Temporal resolution	Spatial resolution	Accuracy (RMSE)
GEWEX/SRB*	3 hourly	1° Global	81.7 Wm ⁻²
EWBMS**	Hourly	0.4° Continental	Undergoing
CER11	Hourly	SSF***	82.7 Wm ⁻²

*: Global energy and water cycle experiment/ Surface radiation budget (http://eosweb.larc.nasa.gov/PRODOCS/srb/readme/readme_srb_rel2_sw_3hrly.txt)
 **: Energy and water balance monitoring system
 ***: Single scanner footprint (Earth observing system data and information system) (http://eosweb.larc.nasa.gov/PRODOCS/ceres/SSF/Quality_Summaries/ssf_surface_flux_terra_ed2B.html)

These products, however, have fine temporal resolution and coarse spatial resolution, which are not appropriate land applications. Routine monitoring (daily to weekly) of surface fluxes is recommended (Kustas et al., 2003; Trnka et al., 2007). In addition, they do not meet the accuracy required by the user community. The required accuracy for surface shortwave downward radiation (S_{\downarrow}) from satellite data is 5 – 10 Wm⁻² at 25 - 100 km (CEOS and WMO, 2000; GCOS, 2006). Several studies have determined the accuracy of S_{\downarrow} estimates in terms of the Root Mean Square Error (RMSE) using surface measurements. RMSE of 109 – 210.9 Wm⁻² are reported at 4

km to 1/8 degree spatial resolution and various time windows (Dedieu et al., 1987; Garatuza-Payan et al., 2001; Pinker et al., 2007; Pinker et al., 2003).

Uncertainty in cloud detection and heterogeneity in surfaces are well-known problems in SRB retrieval. The accuracy estimates listed in Table 1-1 are obtained by comparing the satellite-derived surface shortwave radiation budget with ground point measurements. SRB components can vary on a small spatial scales and land cover can vary on an even finer scale than the atmosphere. A well-established method for validating a coarser-spatial-resolution satellite dataset is to evaluate the higher-spatial-resolution dataset using ground point measurements and use a higher-spatial-resolution dataset to assess the coarse resolution dataset (Goward et al., 2003; Liang et al., 2002). In addition, finer resolution SRB components (up to 1km) have been being studied in numerical climate and ecosystem simulations (Bromwich et al., 2005; Guan et al., 2000; Masson et al., 2003; Soci et al., 2006), however, available SRB products do not support finer spatial resolution models.

1.2 Need for surface net radiation with high spatial resolution

Surface shortwave net radiation (S_n) is required to estimate the energy exchange between the atmosphere and the land/ocean surfaces. It is the fundamental quantity of energy available at the Earth's surface that drives the processes of evaporation, air and soil heating, as well as other, smaller energy-consuming processes such as photosynthesis. S_n is also frequently used to estimate all-wave net radiation (R_n)

(Jacobs et al., 2004; Jacobs et al., 2002; Samani et al., 2007). S_n influences atmospheric circulations as well as surface climate (Whitlock et al., 1995), and is used in numerical weather simulation as well as land surface modeling.

Studies were, however, focused on coarse spatial and spectral resolution satellite data such as Earth Radiation Budget Experiment (ERBE) wide-field-of-view planetary albedo in parameterization (Li et al., 1993b; Masuda et al., 1995) and narrowband radiances of International Satellite Cloud Climatology project (ISCCP) data with a 280 km spatial resolution (Pinker and Laszlo, 1990; Rossow and Zhang, 1995; Zhang et al., 2004). These data are too coarse for recent high-resolution land applications (e.g. ecosystem simulation, energy balance model, land surface model (Kustas et al., 2004; Kustas and Norman, 2000; Kustas et al., 2003; Li et al., 2008; Treitz and Howarth, 2000) as well as numerical climate system (Bromwich et al., 2005; Guan et al., 2000; Masson et al., 2003; Soci et al., 2006). Spatial resolutions less than 10 km were required in those studies.

Nonlinearities in many surface processes often require that models be applied at relatively high spatial and temporal resolution (Marani et al., 1997). Indirect estimates of surface fluxes over extensive areas ($\sim 1^\circ$) based on remote sensing from satellite typically involve treating heterogeneous areas in the same way as the homogeneous areas used to develop the original algorithms. Uncertainties associated with surface and atmosphere heterogeneity are difficult to evaluate because no *in situ* methods exist to measure surface fluxes reliably over such relatively large heterogeneous areas. It is spatial resolution that determines the information content and measurement error of an image (Atkinson, 1993; Atkinson et al., 1996) and that has crucial relevance for

understanding many aspects of the Earth system science (Townshend et al., 1991; 1994).

At such coarse spatial resolution, the capability to monitor the impact of S_n change and disturbances on other parameters such as evapotranspiration or heat flux from different plant (crop) type is severely hampered (Kustas et al., 2004; Kustas and Norman, 2000; Kustas et al., 2003). Landscapes with significant variability in vegetation cover, type/architecture, and moisture, the spatial resolution of the remote sensing data is crucial for discriminating fluxes for the different land cover types and hence avoiding significant errors due to application of a land surface model to a mixed pixel containing large contrast in surface physical parameters (Li et al., 2008; Moran et al., 1997; Zhan et al., 2000). Surface radiation estimation at finer spatial resolution than current products is necessary in order to capture nonlinear surface processes and avoid errors resulting from land surface model application.

The reanalysis data sets are also used in land applications, but they are usually coarse spatial resolutions ($> 1^\circ$) and fine temporal resolutions such as those from NASA Data Assimilation Office (DAO), European Centre for Medium-Range Weather Forecasts (ECWMF, ERA-40), and National Centers for Environmental Prediction and National Center for Atmospheric Research (NCEP/NCAR). Furthermore, there is little known about surface radiation variable accuracies of reanalysis data sets and their impacts on applications (Zhao et al., 2006). It was reported that National Centers for Environment Prediction (NCEP) reanalysis solar radiation data exceeded surface observations more than 100 Wm^{-2} (Xia et al., 2006). The use of reanalysis data from Global Circulation Model (GCM) in land evaporation

algorithm was pointed out as problematic because its accuracy and coarse spatial resolution (Nishida et al., 2003a). Therefore, surface radiation budget dataset with finer spatial resolution are required to support recent land applications.

This study uses Moderate Resolution Imaging Spectroradiometer (MODIS) data to estimate S_n at a 1 km resolution. MODIS is one of the sensors in the National Aeronautics and Space Administration (NASA) Earth Observing System (EOS) Terra platform launched in 1999 and Aqua platform launched in 2002. MODIS provides comprehensive and frequent global Earth imaging in 36 spectral bands (Table 1-2) and at variable spatial resolutions with nadir footprints no greater than 1 km. The new hybrid method presented in this study does not require coarse resolution ancillary data; therefore the hybrid method produces estimated S_n at 1 km resolution.

Previous studies also used narrowband-to-broadband conversion to retrieve parameters. Narrowband-to-broadband conversion was used to retrieve surface albedo and local planetary albedo (Cess et al., 1991; Cess and Vulis, 1989; Frouin and Chertock, 1992; Masuda et al., 1995; Tang et al., 2006). Narrowband to broadband conversions in atmospheric anisotropy have been pointed out as error sources in retrieval techniques (Noia et al., 1993; Perez et al., 2002; Pinker et al., 1995; Schmetz, 1989). In addition, these methods are physically valid at each procedural step; however, the possibility exists that errors associated with each step may cancel or reinforce each other.

Table 1- 2 MODIS spectral band specification

Primary Use	Band	Central wavelength [nm]	Bandwidth [nm]	Spatial resolution [m]
Land / Cloud / Aerosols /	1	645	620 - 670	250
	2	858.5	841 - 876	
Land / Cloud / Aerosols Properties	3	469	459 - 479	500
	4	555	545 - 565	
	5	1240	1230 - 1250	
	6	1640	1628 - 1652	
	7	2130	2105 - 2155	
Ocean Color / Phytoplankton / Biogeochemistry	8	421.5	405 - 420	1000
	9	443	438 - 448	
	10	488	483 - 493	
	11	531	526 - 536	
	12	551	546 - 556	
	13	667	662 - 672	
	14	678	673 - 683	
	15	748	743 - 753	
Atmospheric Water Vapor	16	869.5	862 - 877	
	17	905	890 - 920	
	18	936	931 - 941	
Surface / Cloud Temperature	19	940	915 - 965	
	20	3750	3660 - 3840	
	21	3959	3929 - 3989	
	22	3959	3929 - 3989	
Atmospheric Temperature	23	4050	4020 - 4080	
	24	4465.5	4433 - 4498	
Cirrus Clouds / Water Vapor	25	4515.5	4482 - 4549	
	26	1375	1360 - 1390	
	27	6715	6535 - 6895	
Cloud Properties	28	7325	7175 - 7475	
	29	8550	8400 - 8700	
Ozone	30	9730	9580 - 9880	
Surface / Cloud Temperature	31	11030	10780 - 11280	
	32	12020	11770 - 12270	
Cloud Top Altitude	33	13335	13185 - 13485	
	34	13635	13485 - 13785	
	35	13935	13785 - 14085	
	36	14235	14085 - 14385	

All-wave net radiation (R_n) describes the importance of radiative processes for energy exchange at the Earth's surface and is calculated as the sum of shortwave net radiation (S_n) and longwave net radiation (L_n).

$$R_n = (S_{\downarrow} - S_{\uparrow}) + (L_{\downarrow} - L_{\uparrow}) = S_n + L_n \quad (1-1)$$

where S_{\uparrow} is shortwave upward radiation, L_{\downarrow} is longwave downward radiation, and L_{\uparrow} is longwave upward radiation.

Estimated R_n is often used because R_n measurements are very rare. If meteorological datasets are used, it is necessary to validate the calibration coefficients locally. When satellite data are used, numerous parameters, such as cloud fraction, cloud base temperature, clear air emissivity, and surface temperature, must be retrieved to calculate longwave net radiation (L_n) and errors associated with each procedure are unknown to cancel or reinforce each other. In addition, cloud top temperature is used to estimate R_n instead of cloud base temperature, because it is currently impossible to retrieve cloud base temperature from satellite data. Also, ancillary data with different spatial resolutions are required to retrieve these parameters. Cloudy-sky R_n estimation with 1 km resolution has not been reported yet although modeling community requires it (Bromwich et al., 2005; Guan et al., 2000; Masson et al., 2003; Soci et al., 2006). Method to estimate cloudy-sky R_n at 1 km spatial resolution is developed in this study.

Daily integrated shortwave net radiation (S_n) at the Earth surface is a fundamental driving variable for simulation of ecosystem carbon, water, and energy fluxes at local, regional, and global scales. Meteorological and astronomical datasets are often used, however, they are spatially limited. Monthly averaged data are produced when satellite-based datasets are used, however, these averaged data eliminate the exact sequence of cold-or-warm, wet-or-dry days that is an important factor in processes such as vegetation net primary production (Hunt et al., 1991). Therefore, the method for estimating daily integrated S_n from instantaneous S_n values at 1 km resolution is presented in this study.

1.3 Objectives of this study

The overall goal of this study is to develop algorithms that estimate surface all-sky shortwave net radiation (S_n) and cloudy-sky all-wave net radiation from the MODIS data at a high spatial resolution. The definition of high resolution varies depending on the times and applications. The applications considered in this study are land surface models, numerical weather prediction models, and ecosystem simulations, and they require a finer spatial resolution than existing products.

The first objective of this study is to develop an algorithm to estimate instantaneous S_n directly from MODIS Top-Of-Atmosphere (TOA) and surface spectral reflectance at finer spatial resolution. This algorithm is composed of two parts: 1) a physical part that simulates surface spectral flux and TOA reflectance

using radiative transfer code MODerate resolution atmospheric TRANsmission version 4 (MODTRAN4) radiative transfer code, and 2) a statistical part that links simulated S_n and TOA and surface reflectance. New hybrid algorithm is straightforward and does not require coarse resolution ancillary data; therefore it is irrelevant to errors in parameter retrievals and raw input resolution is retained.

The second objective is to estimate cloudy-sky all-wave net radiation (R_n) from S_n and to take into consideration surface characteristics. R_n is sum of S_n and longwave net radiation (L_n) and previous studies have documented the close relationship between R_n and S_n (Diak and Gautier, 1983; Gautier et al., 1980; Ma et al., 2002). Difficulty in estimating cloudy-sky longwave net radiation, however, has been reported (Ellingson, 1995). R_n is closely related to vegetation type and state because vegetation type and state partly determine the fraction of net radiation used for evapotranspiration, photosynthesis, and respiration rates. Cloudy-sky R_n , therefore, can be estimated by using S_n and vegetation type and status. Ground measurement data and surface type are used to generate empirical formulae and the Earth's surface is characterized with Enhanced Vegetation Index (EVI) and Plant Functional Types (PFT). Estimating cloudy-sky R_n from this method overcomes the limits in spatial coverage of measured R_n and enables estimation of all-sky R_n at finer spatial resolution, because the clear-sky longwave net radiation from MODIS data is recently estimated with greater accuracy than pre-existing products (Wang and Liang, 2008).

The third objective is to produce daily integrated S_n . Many land surface models require integrated S_n at a daily temporal resolution (Alexandrov and Hoogenboom, 2000; Chen et al., 2007; Wolf et al., 1996). Previous studies have used air temperature, other meteorological data sets, or simply substituted data from the closest station to estimate daily integrated S_n (Fletcher and Moot, 2007; Hunt et al., 1998; Rivington et al., 2005; Wu et al., 2007). The variation of S_n during the course of a day is similar to that of photosynthetically active radiation (PAR) (found in ground measurement data), therefore, adjusted sinusoidal interpolation for daily-PAR integration method is adapted. Adjusted sinusoidal interpolation can be also applied to daily integrated R_n .

The proposed study has the potential to provide three contributions to the scientific community. First, the study will produce S_n at finer spatial resolution with comparable accuracy to existing SRB products. Finer spatial resolution of S_n will capture the specific sequence of the redistribution of the available energy at the Earth's surface. As the result and secondly, S_n derived from this study can support high resolution numerical weather prediction and land surface models. Finally, a finer spatial resolution S_n will more accurately assess existing coarse-spatial-resolution SRB datasets.

Chapter 2: Estimating Shortwave Net Radiation Using MODIS Data

The relationship between the solar atmospheric transmittance and the reflected radiation field at the top of the atmosphere is affected by the solar zenith angle, gaseous and aerosol absorption and scattering, surface reflectivity and clouds. The retrieval of SRB from satellite-observed radiation crucially depends on whether the atmospheric absorption can be estimated with sufficient accuracy (Schmetz, 1989).

Surface downward radiation is influenced mainly by the atmospheric properties, but also to a lesser extent by surface reflectance. It is the integration of spectral flux for shortwave region and can be demonstrated by the following equation:

$$F_d(\mu_0) = \int_{\lambda_1}^{\lambda_2} F_\lambda(\mu_0) d\lambda \quad (2-1)$$

where $F_d(\mu_0)$ is downward solar radiation, λ is wavelength, λ_1 and λ_2 is the spectral range of shortwave radiation (0.3 – 3 μm), μ_0 is $\cos(\theta_0)$ at the solar zenith angle θ_0 . Spectral downward radiation, $F_\lambda(\mu_0)$, can be expressed as (Liang, 2004):

$$F_\lambda(\mu_0) = F_0(\mu_0) + \frac{\bar{r}_s \bar{\rho}}{1 - r_s \rho} \mu_0 E_0 \gamma(\mu_0) \quad (2-2)$$

where $F_0(\mu_0)$ is the downward flux without any contribution from the surface, r_s is surface reflectance, $\bar{\rho}$ is spherical albedo of the atmosphere, E_0 is the extraterrestrial solar irradiance, and $\gamma(\mu_0)$ is total transmittance (direct and diffuse) in the solar illumination direction. The left side of Equation 2-2 represents the surface flux. The first term on the right side of the equation is the sum of the direct and diffuse flux and the second term is related to multiple scattering.

Atmospheric properties can be explained by scattering and absorption. The optical properties (e.g. optical depth, single scattering albedo, phase function) of the medium are determined by the particles that compose the medium and their properties. If the molecular particles in the atmosphere are far smaller than the wavelength, its scattering pattern can be calculated by the Rayleigh scattering. If the particle size is very close to the length of wavelength, such as most aerosol particles in the atmosphere, their scattering behavior can be characterized by Mie scattering. Aerosols have a shortwave cooling effect at the surface level under clear-sky condition and warming effect under cloudy-sky condition (Li and Trishchenko, 2001). At TOA, aerosols have a shortwave warming effect due to enhanced absorption under cloudy-sky condition and a cooling effect under clear-sky condition which are 3 – 4 times less than that at the surface level.

Molecular or Rayleigh scattering is more important at shorter wavelengths where the solar contributions dominate. MODTRAN models the single scatter solar radiation accounting for the solar spectrum (Kurucz, 1992; 1994), the curvature of the Earth, refractive geometry effects (Ridgway et al., 1982; Callery et al., 1983; Kneizys et al., 1983), and a general scattering phase function. Multiple scattering, which is

much more difficult to treat accurately, is handled with a plane-parallel atmospheric approximation (Andersson, 1982) and a Henyey-Greenstein phase function. Rayleigh scattering transmittance also depends on the elevation-related airmass, which are not taken into account in radiative transfer simulation, it is considered in section 2.2.4.

Absorption is caused mainly by atmospheric gases, such as water vapor, ozone, and oxygen, as well as aerosols. The most variable gas that significantly affects remotely sensed data is water vapor. It is found mostly in the boundary layer and water vapor content varies between 0.42 gcm^{-2} in sub-arctic regions in winter and 4.12 gcm^{-2} in tropical regions (Liang, 2004). Even daily fluctuation from 1.0 to 4.0 gcm^{-2} has been reported (Holben and Eck, 1990), therefore daily transmittance related to water vapor is considered in this study (section 2.2.3). Water vapor absorbs solar radiation in the wavelength larger than $0.5 \mu\text{m}$ and has a shortwave cooling effect at the surface level under both clear- and cloudy-sky condition (Li and Trishchenko, 2001).

Major factors affecting downward fluxes under clear-sky condition are aerosol and water vapor as well as solar zenith angle. Clouds are the strongest modulators of the shortwave radiation fields (Wielicki et al., 1998). Clouds absorb in the near infrared, which reduces the water vapor absorption below the cloud since cloud reflection and absorption shield the lower levels. Due to this compensation between cloud and water vapor absorption, the total absorption of clouds and gases is not changed drastically by clouds (Ramanathan, 1986; Schmetz, 1989). It is, however, not possible to measure the background clear-sky fluxes under cloudy-sky condition, determination of the clear-sky reference value is one of the major sources of

uncertainty in SRB estimation under cloudy-sky condition (Pinker et al., 1995). In order to reduce this uncertainty, both clear and cloudy-sky conditions were considered in each angular bins by using statistical method in this study.

The radiative transfer model (MODTRAN4) accounts for absorption by ozone and water vapor, multiple scattering by molecules, multiple scattering and absorption by aerosols and cloud droplets, and multiple reflection between the atmosphere and surface. The vertical profiles of ozone and water vapor densities, temperature, and pressure are those of the standard atmospheres (tropical, midlatitude summer and winter, sub-arctic winter and summer) (Berk et al., 2003).

2.1 Existing methods for surface shortwave net radiation estimates

Although some statistical methods estimate surface shortwave net radiation (S_n) by establishing the regression relation between satellite-measured brightness and S_n measurement (Cano et al., 1986; Hay and Hanson, 1978; Tarpley, 1979), many studies estimate shortwave net radiation (S_n) using TOA radiance, atmospheric and surface variables (Cess et al., 1991; Cess and Vulis, 1989; Li et al., 1993a; Pinker et al., 1985; Pinker and Laszlo, 1992; Rossow and Zhang, 1995; Tang et al., 2006; Zhang et al., 2004). The current method retrieves parameters relevant to S_n with a radiative transfer model. A set of parameters with a proper degree of increment should be taken into account to get a high degree of accuracy, which might lead computational load. Solar zenith angle and atmospheric water vapor were found significant factors to influence S_n and modest aerosol correction was required for

clear sky (Cess and Vulis, 1989). Detailed parameterization of atmospheric properties, including surface elevation (surface pressure), ozone amount, aerosol type and amount, and cloud height and type (characterized by cloud droplet radius), produced more accurate estimates of S_n (Masuda et al., 1995).

Li et al (1993a) suggested a S_n estimation method based on radiative transfer model simulation:

$$S_n = \alpha(\mu, p) - \beta(\mu, p)r \quad (2-3)$$

where μ is the cosine of the solar zenith angle, p is precipitable water, and r is local planetary albedo. Intercept α and slope β are calculated with Equations 2-4 and 2-5:

$$\alpha(\mu, p) = \alpha_0(\mu) + \frac{1}{\mu} [1 - \exp(-\mu)] (0.0699 - 0.0683\sqrt{p}) \quad (2-4)$$

$$\beta(\mu, p) = \beta_0 - 0.0273 + 0.0216\sqrt{p} \quad (2-5)$$

The CERES single-scanner footprint (SSF) surface fluxes product uses this method to produce clear-sky S_n (Wielicki et al., 1998). Recently, Tang et al (2006) adopted this parameterization scheme and presented variable slope and intercept constants depending on various surface covers (land, ocean and snow/ice). They suggested a narrowband-to-broadband albedo conversion equation to calculate local planetary albedo (TOA albedo). The linear conversion formula (Tang et al., 2006) used in local planetary albedo (r) is:

$$r = b_0 + b_1\rho_1 + b_2\rho_2 + b_3\rho_3 + b_4\rho_4 + b_5\rho_5 + b_6\rho_6 + b_7\rho_7 \quad (2-6)$$

where ρ_i is TOA narrowband reflectance of MODIS band i and b_i is a coefficient calculated from the function of the viewing zenith angle (VZA):

$$b_i = c_{1i} + c_{2i} / (1 + \exp((1 / \cos(VZA) - c_{3i}) / c_{4i})) \quad (2-7)$$

where $c_{1i} - c_{4i}$ are constants for a given solar zenith angle.

These methods, however, convert TOA radiance to broadband flux, then surface shortwave net radiation is linked. Detailed indications about atmospheric and surface properties in multispectral data can be lost in this process. Also, errors associated with retrieving each required parameters are unknown to cancel or reinforce each other. Estimating these parameters may be more challenging than estimating surface net radiation.

Another issue related to existing methods is inconsistency in the spatial and resolution of ancillary data as well as suitability to coarse resolution data. ISCCP global data, for example, are produced by merging the analyses of narrowband radiances measured by the network of weather satellites with the TIROS operational vertical sounder (TOVS) daily analysis product produced by National Oceanic and Atmospheric Administration (NOAA) and some ancillary data (Zhang et al., 1995). The main ancillary data sets are: land/water fraction and the mean topography at a resolution of 25 km, the surface/vegetation type at a resolution of about 100 km, and the weekly snow/ice cover data from NOAA/National Environmental Satellite data

and Information Service (NESDIS) and United States Navy/NOAA Joint Ice Center (Rossow and Schiffer, 1991). Moreover, geostationary satellites have limited use at high latitude regions due to their restricted viewing geometry.

2.2 Theoretical basis of the new hybrid algorithm

All-sky surface shortwave net radiation (S_n) is estimated from TOA reflectance using a hybrid algorithm at 1 km spatial resolution. The first step is to simulate MODIS TOA reflectance and shortwave net radiation (S_n) with the MODIS spectral response function and surface reflectance spectra. The second step uses statistical techniques to establish the relationship between S_n and MODIS TOA reflectance. A flowchart of the hybrid S_n algorithm is shown in Figure 2-1.

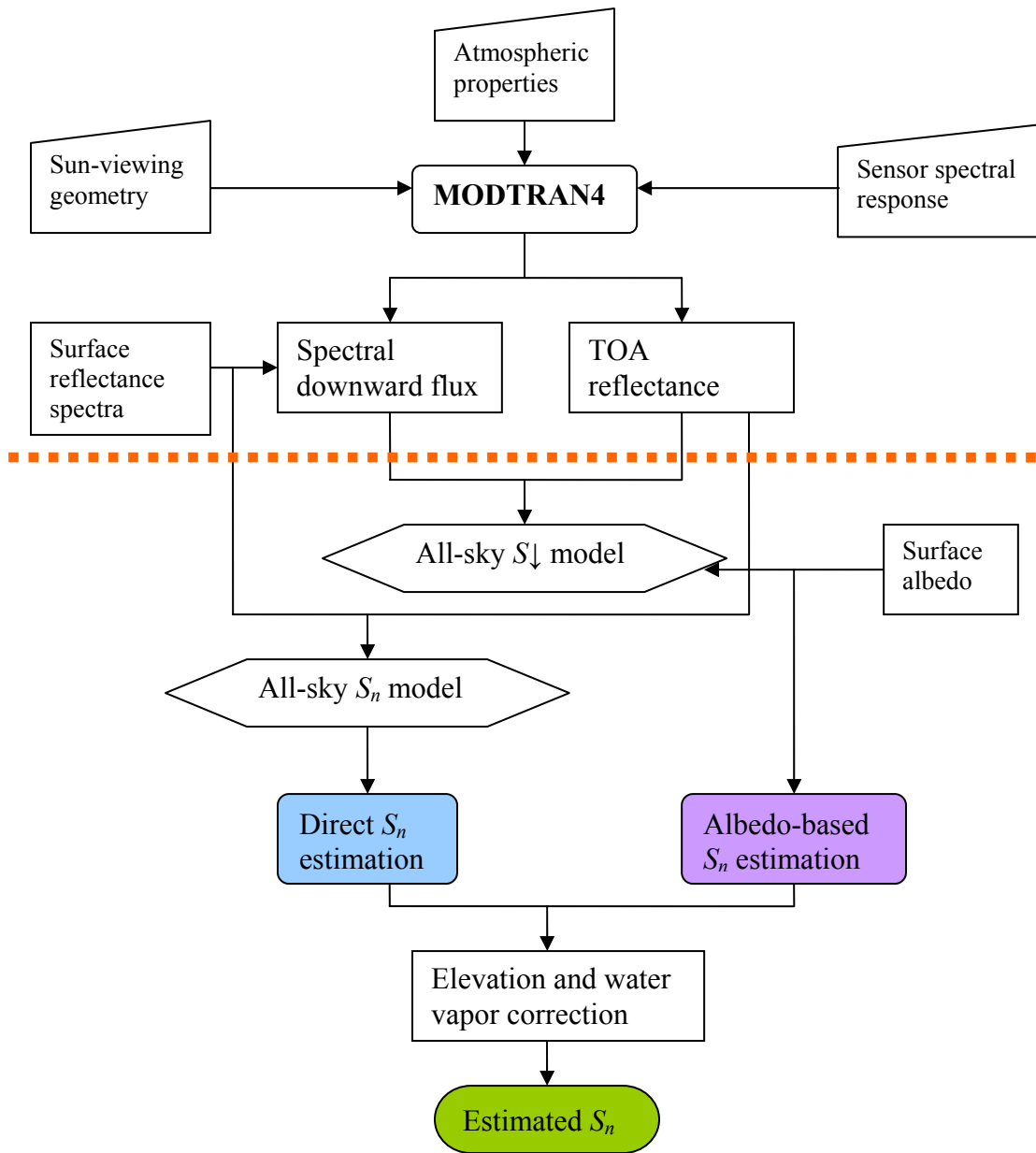


Figure 2- 1 Flowchart depicting the hybrid algorithm for shortwave net radiation estimation. Above the dashed red line indicates physical part of the hybrid algorithm and below indicates statistical part of the hybrid algorithm

2.2.1 Radiative transfer simulation

MODerate resolution atmospheric TRANsmission version 4 (MODTRAN4) was used to simulate spectral downward flux and MODIS TOA radiances for known solar zenith angle and atmospheric conditions (e.g., visibility, aerosol type) (Berk et al., 1999). Nine solar zenith angles (0°, 20°, 40°, 50°, 60°, 65°, 70°, 75°, and 80°) and seven different visibilities (5, 10, 20, 30, 50, 100, and 1000 km) were used in the clear-sky simulation, and four types of cloud were used in the cloudy-sky simulation. Five viewing zenith angles (0°, 15°, 30°, 45°, and 65°) and seven relative azimuth angles (0°, 30°, 60°, 90°, 120°, 150°, and 180°) were added to create total 315 angular bins to characterize the Sun-satellite geometry for the MODIS TOA radiance simulation.

Downward spectral flux at a Lambertian surface at the solar zenith angle (θ_0) can be calculated using Equation 2-2.

$$F(\mu_0) = F_0(\mu_0) + \frac{\bar{r}_s \bar{\rho}}{1 - \bar{r}_s \bar{\rho}} \mu_0 E_0 \gamma(\mu_0) \quad (2-2)$$

Solving Equation 2-2 for three surface reflectance specifications (0.0, 0.5, and 0.8) provides the values of the unknown atmospheric parameters. Downward spectral flux was integrated to represent shortwave downward radiation ($S\downarrow$). $S\downarrow$ is used in albedo-based estimation in Figure 2-1. Surface shortwave upward radiation ($S\uparrow$) was calculated by multiplying surface reflectance spectra to surface downward radiation

(S_{\downarrow}) and S_n was calculated as the difference between S_{\downarrow} and S_{\uparrow} . S_n is used in the direct estimation in Figure 2-1.

Equation 2-8 (Liang, 2004) were used to obtain the TOA radiance at viewing zenith angle (θ).

$$I(\mu_0, \mu, \phi) = I_0(\mu_0, \mu, \phi) + \frac{r_s}{1 - r_s \rho} \mu_0 E_0 \gamma(-\mu_0) \gamma(\mu) \quad (2-8)$$

where $I(\mu_0, \mu, \phi)$ is upward TOA radiance, $\mu = \cos(\theta)$, ϕ is the relative azimuth angle, $I_0(\mu_0, \mu, \phi)$ is path radiance without surface contributions, and $\gamma(\mu)$ is the total transmittance from the surface to the sensor. All surfaces are assumed to be Lambertian reflectors.

2.2.2 Linking TOA reflectance and shortwave net radiation

Parametric and nonparametric statistical techniques, such as multivariate linear regression and Artificial Neural Network (ANN), were used to model the relationship between MODIS TOA reflectance and surface shortwave net radiation (S_n).

TOA radiance is transformed into equivalent reflectance by normalizing the solar irradiance at TOA using Equation 2-9 where the Earth-Sun distance in astronomical units is assumed to be one:

$$\rho_{TOA} = \frac{I(\mu_0, \mu, \phi) \cdot \pi}{\cos(\theta_0) \cdot E_0} \quad (2-9)$$

where I is TOA radiance, θ_0 is the solar zenith angle, and E_0 is solar spectral irradiance (Thuillier's data (http://oceancolor.gsfc.nasa.gov/DOCS/RSR/Thuillier_F0.dat) were used in the present study).

Multivariate linear regression was performed for each angular bin to establish the relationship between S_n and MODIS TOA and surface reflectance using Equation 2-10.

$$S_n(\theta_0, \theta, \phi) = a_{\theta_0, \theta, \phi} + \sum_{i=1}^7 b_{i, \theta_0, \theta, \phi} \cdot \rho_{TOA_i, \theta_0, \theta, \phi} + \sum_{i=1}^7 c_{i, \theta_0, \theta, \phi} \cdot \rho_{S_i, \theta_0, \theta, \phi} \quad (2-10)$$

where θ_0 is the solar zenith angle, θ is the viewing zenith angle, ϕ is the relative azimuth angle; $a_{\theta_0, \theta, \phi}$, $b_{i, \theta_0, \theta, \phi}$, and $c_{i, \theta_0, \theta, \phi}$ are regression coefficients estimated using multivariate regression, i represents MODIS bands in the shortwave region (1 – 7), $\rho_{TOA_i, \theta_0, \theta, \phi}$ and $\rho_{S_i, \theta_0, \theta, \phi}$ indicates TOA and surface reflectance respectively. Each angular bin produced contains all-sky condition data that includes both clear- and cloudy-sky simulations. Linking between S_n and TOA and surface reflectance was also performed with an ANN approach by using Neuroet1 software (Noble and Tribou, 2007). The Neuroet1 scheme is shown in Figure 2-2. The inputs to the ANN were the simulated S_n and TOA and surface reflectance in MODIS band 1 – 7.

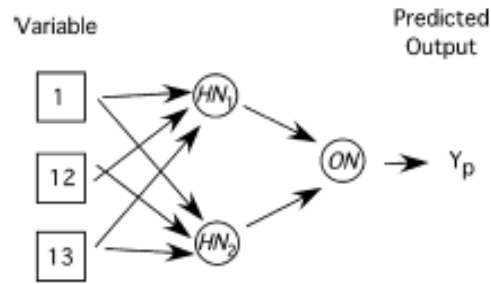


Figure 2- 2 Scheme showing the relationship between variable, hidden neurons (HN), output neurons (ON), and predicted outputs (Y_p) (adapted from Noble and Tribou, 2007)

ANN is adjusted, or trained, so that a particular input leads to a specific target output. This situation is shown in Figure 2-3. The network is adjusted, based on a comparison of the output and the target, until the network output matches the target. Many input/target pairs are needed to train a network.

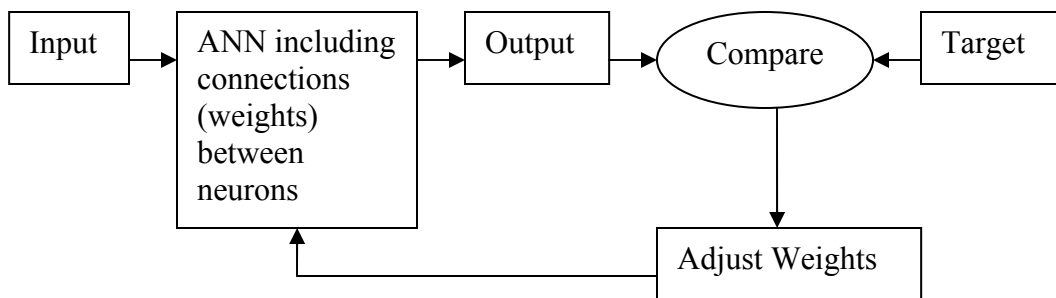


Figure 2- 3 ANN working scheme

2.2.3 Water vapor correction

The uncertainty in Surface Radiation Budget (SRB) components estimation is due in part to the uncertainty in water vapor content (Cess et al., 1995; Forster and

Gregory, 2006; Zhang et al., 2004). The default water vapor amount was set in radiative transfer simulations. One way of considering water vapor effect is to input simulated water vapor amount in regression. Normalized water vapor transmittance coefficient was used in this study to reduce simulation and computation time.

There are many models for calculating water vapor transmittance (Annear and Wells, 2007). Three equations were compared in this study. The water vapor transmission coefficient (T_w) can be calculated by using 1) Duchon and O'Malley's (1999), 2) Bird and Hulstrom (1981), and 3) a fitted method (Wang, 2008).

The water vapor transmission coefficient in Duchon and O'Malley's (1999) method is calculated as:

$$T_w = 1 - 0.077 \cdot (u \cdot m)^{0.3} \quad (2-11)$$

where u is water vapor amount in cm and m is atmospheric mass at surface. The optical air mass number (m) at 101.3 kPa is calculated with Equation 2-12.

$$m = \frac{35}{\sqrt{1224 \cdot \cos(\theta_s)^2 + 1}} \quad (2-12)$$

where θ_s is solar zenith angle

Bird and Hulstrom (1981) calculated the transmittance of the water vapor as

$$T_w = 1 - \frac{2.4959 \cdot (u \cdot m)}{(1 + 79.034 \cdot (u \cdot m))^{0.6828} + 0.6385 \cdot (u \cdot m)} \quad (2-13)$$

Wang (2008) suggested Equation 2-14 based on the radiative transfer simulation and model fitting.

$$T_w = \sqrt{0.8197 - 0.07066 \cdot \lg(u \cdot m)} \quad (2-14)$$

After water vapor transmittance is calculated, water vapor is normalized. Normalized water vapor transmittance is defined as:

$$C_w = \frac{T_w(u, m)}{T_{wd}(u_d, m)} \quad (2-15)$$

where $T_w(u, m)$ is water vapor transmittance for water vapor amount u in cm, which is extracted from MOD05_L2 and $T_{wd}(u_d, m)$ is water vapor transmittance at a default setting simulation.

All three methods were applied and results are summarized in Table 2-1. Methods did not show big difference. RMSEs were reduced after water vapor correction by 0.93% (Wang), 0.83% (Duchon and O'Malley's), and 0.80% (Bird and Hulstrom). Wang (2008) method, which shows best improvement, was applied to this study.

Table 2- 1 Comparison of water vapor transmission calculation

Methods	RMSE reduction (%)	Bias reduction (%)
Wang (2008)	0.93	0.48
Duchon and O'Malley's (1999)	0.83	0.29
Bird and Hulstrom (1981)	0.80	0.31

2.2.4 Elevation correction

Elevation was set to zero meters in radiative transfer model simulations. Surface elevation controls the atmospheric mass that in turn affects Rayleigh scattering transmittance; therefore, I examined the difference between current radiative transfer model simulation (sea level setting) and simulations with variable elevation settings of 0.5km, 1 km, 1.5 km, 2 km, 3 km, 4 km, and 5 km. To quantify elevation effect, normalized transmittance can be defined as:

$$T_n = \frac{T_{ray,z}}{T_{ray,0}} \quad (2-16)$$

where $T_{ray,z}$ is the Rayleigh scattering transmittance at an elevation z in km and $T_{ray,0}$ is the Rayleigh scattering transmittance at sea level. The application of this method to the PAR elevation correction reduced error (Wang et al., 2008b). Surface elevation data can be downloaded from GTOPO30 at a spatial resolution 30 arc seconds (<http://edc.usgs.gov/products/elevation/gtopo30/gtopo30.html>). Fig. 2-4 shows the variation of normalized elevation coefficients with elevation and solar zenith angle.

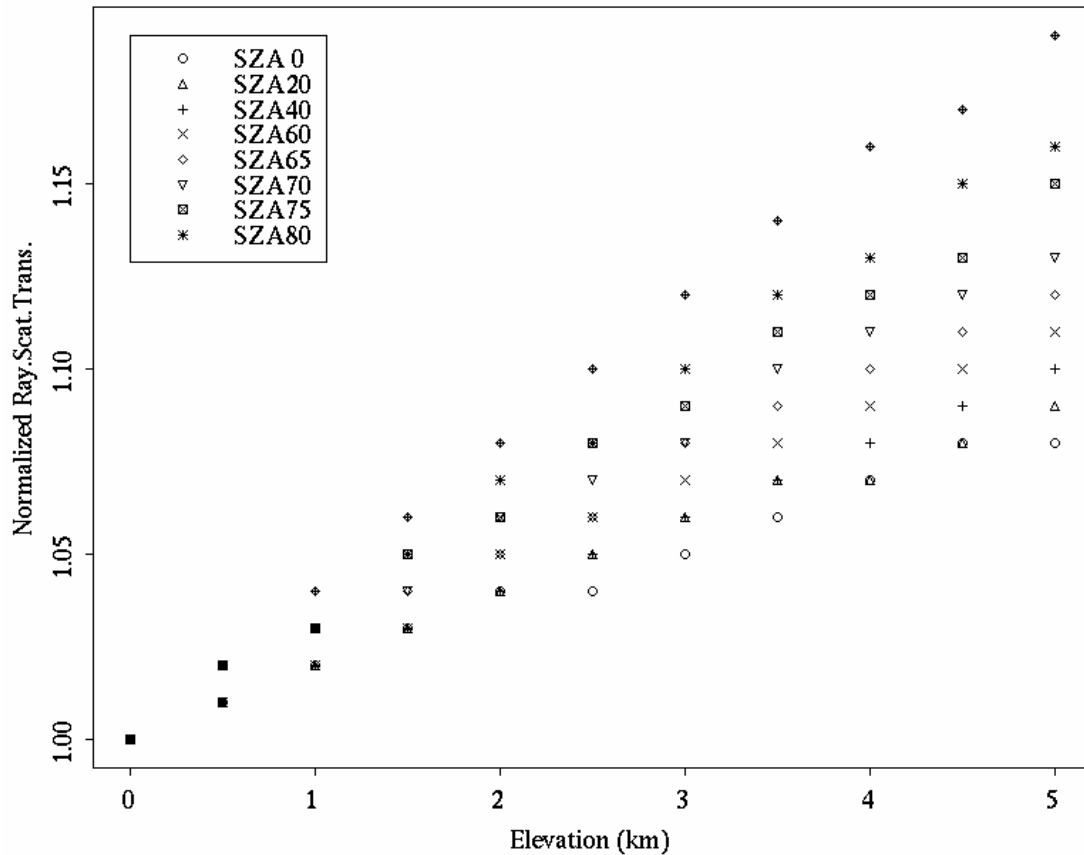


Figure 2- 4 Normalized elevation coefficients depending on solar zenith angle

2.3 Data sets

A variety of data sets were used in this study to develop and evaluate methods for shortwave net radiation (S_n) estimation. The direct estimation method required representative surface reflectance spectra to calculate S_n as well as MODIS TOA and surface reflectance data. The MODIS albedo data were used for the albedo-based estimation method. Surface measurements were used for evaluation.

2.3.1 Surface reflectance spectra

S_n is highly related to surface characteristics; therefore, calculating S_n requires representative surface reflectance spectra. Two hundred fifty-six surface reflectance spectra were used to calculate S_n . One hundred twenty spectra were obtained from the United States Geological Survey (USGS) spectral library (<http://speclab.cr.usgs.gov/>) and Dr. Shunlin Liang provided the rest of spectra.

2.3.2 MODIS products

TOA reflectance was obtained from two MODIS level 1B dataset: MOD021KM and MOD03. The MOD021KM product is calibrated Earth View data at 1 KM resolution by the MODIS Characterization and Support Team (MCST), with including the 250 m and 500 m resolution bands aggregated to appear at 1 km resolution. The MOD021KM products are TOA radiance and reflectances (Toller et al., 2006). The first seven spectral bands (Table 1-3) of the MOD021KM were used. These channels were selected to consider dominant insolation, aerosol, cloud, and water vapor effects in SRB. The MOD03 products consist of geolocation fields data calculated for each 1 km MODIS Instantaneous Field of View (IFOV). The geolocation fields include geodetic latitude, longitude, surface height above the geoid, solar zenith and azimuth angles, satellite zenith and azimuth angles, and a land/sea mask for each 1 km sample.

Water vapor amount was acquired from the MODIS level 2 dataset: MOD05_L2. The MOD05_L2 products are the near-infrared total precipitable water data consisting of column water vapor amounts over clear land areas of the globe, and above clouds over both land and ocean. MODIS level 1 and 2 data sets are downloadable from Level 1 and Atmosphere Archive and Distribution System (LAADS web, <http://ladsweb.nascom.nasa.gov>).

Surface albedo information was acquired from the MODIS Bidirectional Reflectance Distribution Function (BRDF)/Albedo product: MOD43B3. The MODIS global albedo is operationally produced every 16 days at a 1 km spatial resolution. The product is derived in seven spectral bands, as well as in the visible, the near/mid-infrared and the total shortwave broadbands (Schaaf et al., 2002). The product provides the completely diffuse bihemispherical (white-sky albedo) and directional hemispherical reflectance (black-sky-albedo). Directional hemispherical reflectance in total shortwave broadbands was used in the study.

Surface reflectance data was obtained from the MODIS surface reflectance grid data: MOD09GHK. The MOD09GHK is a seven-band product computed from MODIS level 1B land bands 1 – 7 and provides daily surface reflectance. Data sets are available in Land Processes Distributed Active Archive Center (LP DAAC, <http://edcimswww.cr.usgs.gov/pub/imswelcome/>)

2.3.2 Surface measurements

The Surface Radiation Budget Network (SURFRAD) was established in 1993 to support climate research with accurate, continuous, long-term measurements of the surface radiation budget over the United States. Seven stations are currently operating and provide global solar radiation (0.28 – 3 μm) with three minute intervals (Augustine et al., 2005). Figure 2-5 shows the seven operating sites. Table 2-1 summarizes site location information.

Figure 2- 5 Seven SURFRAD sites



Table 2- 2 Location of SURFRAD sites

Station	Short Name	Latitude	Longitude	Elevation(m)
Bondville, IL	BON	40.05	- 88.37	213
Boulder, CO	TBL	40.13	- 105.24	1689
Desert Rock, NV	DRA	36.63	- 116.02	1007
Fort Peck, MT	FPK	48.31	-105.10	634
Goodwin Creek, MS	GWN	34.25	- 89.87	98
Penn State, PA	PSU	40.72	- 77.93	376
Sioux Falls, SD	SXF	43.73	- 96.62	473

2.4 Validation

Validation is the process of determining the degree to which an estimated products/model provides an accurate representation of the real world (Justice et al., 2000; Salomon et al., 2006). Independent field measurements on the ground or from a tower are generally presumed to be “ground truth” and are often taken as the reference for validation. While independent field measurements are typically only representative of small areas on the Earth, they remain the primary source of ground truth data for validation of the estimated products. One of problems in validation of estimated products from remotely sensed data is the scale mismatch between ground point measurement and satellite measurements because a single satellite measurement can measure energy from a very large area relative to field measurements (Wang et al., 2004a).

When land surface is heterogeneous, a number of ground measurements are needed to capture spatial variance of the surface radiation and hence to represent the mean radiation value over the region covering a satellite pixel. This, however, poses both logistic and practical difficulties for validation (Tian et al., 2002). An alternative is to select relatively homogeneous regions for the validation so that the ground measurement matches well the mean radiation at the satellite scale. The Surface Radiation Budget Network (SURFRAD) (Augustine et al., 2005) were designed to provide accurate and continuous measurements of the surface radiation budget and the landform and vegetation are relatively homogeneous over an extended region around stations. Upward and downward radiation measurements are routinely

measured at a temporal resolution of 3 minutes, from which the surface net radiation can be calculated. Therefore, SURFRAD sites can provide ground observation to verify the satellite-based radiation retrievals. Intercomparison of data products or model outputs provides an initial indication of differences and possibly insights into the reasons for the differences (Justice et al., 2000), therefore, comparisons with GEWEX/SRB and ISCCP data are included in this chapter.

Hybrid methods developed in this study were evaluated at seven SURFRAD sites. Surface radiation budget product is primary input to numerous applications and its uncertainty could affect the application result, to determine product accuracy is necessary step. The three-minute surface measurements used for validation were those closest to satellite overpass time.

2.4.1 Hybrid algorithm: Direct estimation

All-sky shortwave net radiation (S_n) was estimated using the hybrid algorithms. Multivariate linear regression and Artificial Neural Network (ANN) methods were used to link S_n and TOA and surface reflectances. Estimated S_n for the year 2005 was compared to the surface measurement data collected at the seven SURFRAD sites. A total of 315 angular bin models were developed and evaluated with the multivariate linear regression and ANN methods to determine the most effective approach. ANN methods showed better fitting results as shown in Figure 2-6, however, multivariate linear regression estimates surface measurements more accurately in validation in terms of correlation coefficients and Root Mean Squared Error (RMSE). For ANN, it

is easy to get a good or excellent result on the in-sample data, but this by no means suggests that a good model is found. This overfitting limits the generalization ability of predictive models (Zhang, 2007). Therefore, multivariate linear regression was used in remainder of the study.

Figure 2-7 compares estimated S_n using multivariate linear regression and surface measurements collected closest to the satellite-overpass time. Multivariate linear regression estimates S_n with RMSEs of 74.9 – 110.9 Wm^{-2} . Table 2-3 summarizes the validation results.

Table 2- 3. Validation of estimated shortwave net radiation using hybrid method (direct estimation) at 1-km and time closest to satellite overpass

Sites	R²	RMSE (Wm^{-2})	Bias (Wm^{-2})
BON	0.8357	88.4	-1.4
TBL	0.7616	110.9	-45
GWN	0.8029	94.5	2.9
DRA	0.8111	74.9	-51.8
FPK	0.8277	93.7	-24.1
PSU	0.7915	107.3	13.2
SXF	0.8442	86.7	-6.2
mean	0.8107	93.8	-16.1

Figure 2- 6 Simulated shortwave net radiation fitting using multivariate linear regression (top) and artificial neural network (bottom)

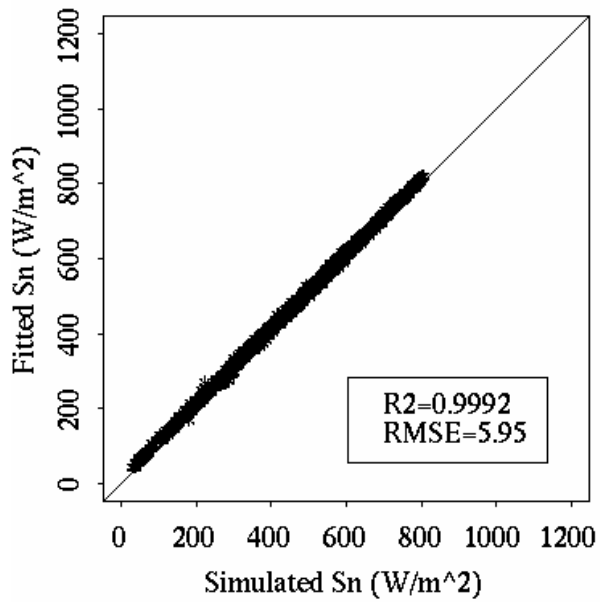
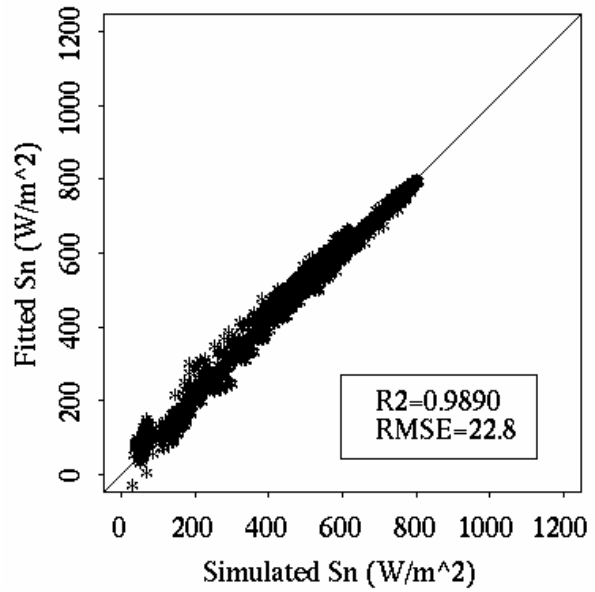
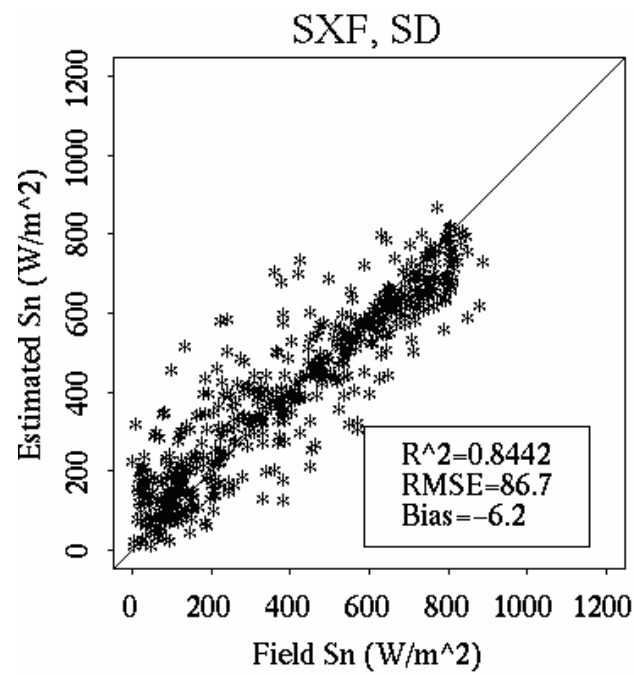
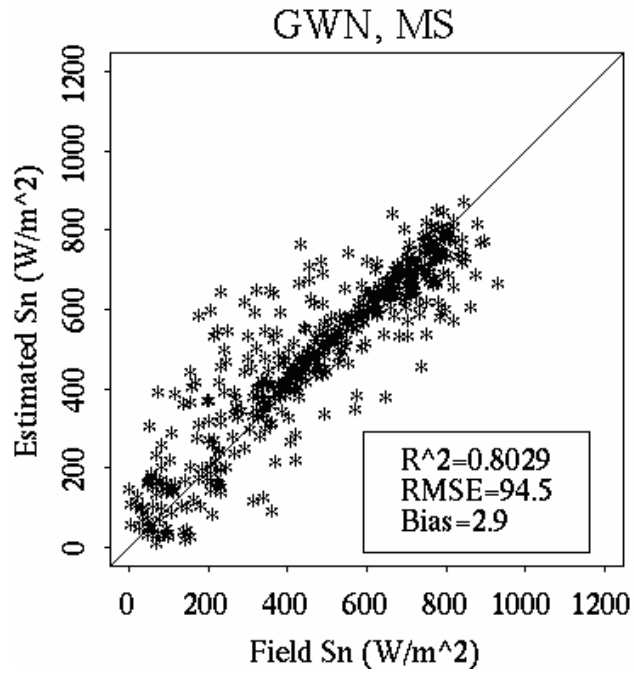


Figure 2- 7 Validation of shortwave net radiation estimation using hybrid method (direct estimation) for the SURFRAD sites



2.4.2 Hybrid algorithm: Albedo-based estimation

Surface shortwave net radiation (S_n) can be calculated with surface albedo (α).

$$S_n = S\downarrow(1 - \alpha) \quad (2-17)$$

Surface downward radiation ($S\downarrow$) was obtained from the MODTRAN4 simulation and surface albedo was extracted from the standard MODIS albedo product. The standard MODIS albedo products have generally been used as a reference data set to evaluate the results from climate models (Roesch and Roeckner, 2006; Wang et al., 2004b; Zhou et al., 2003) and land surface albedo products from other sensor such as Multi-angle Imaging SpectroRadiometer (MISR) (Chen et al., 2008). Spatially continuous MODIS albedo products developed by using temporal scaling filter was applied to generate ultraviolet albedo (Kim et al., 2008).

Figure 2-8 shows the validation results and the results are summarized in Table 2-4. A large RMSE is noticed in Table 2-4. The variation in temporal resolution between the albedo product and estimated shortwave downward radiation ($S\downarrow$) as well as spatial differences between satellite data and surface measurements are suspected as major sources of error. The MODIS albedo product is produced in 16 days to obtain enough number of observations to calculate surface albedo and it is not retrieved if there is lack of observations to calculate albedo due to cloud cover, seasonal snow, and/or instrument problems (Fang et al., 2007). Same albedo value was used more than 16 days in albedo-based estimation if there were no available

surface albedo. S_{\downarrow} , on the other hand, can be estimated daily if satellite observation is available.

Figure 2- 8 Validation of shortwave net radiation estimation using hybrid method (albedo-based estimation) for SURFRAD sites

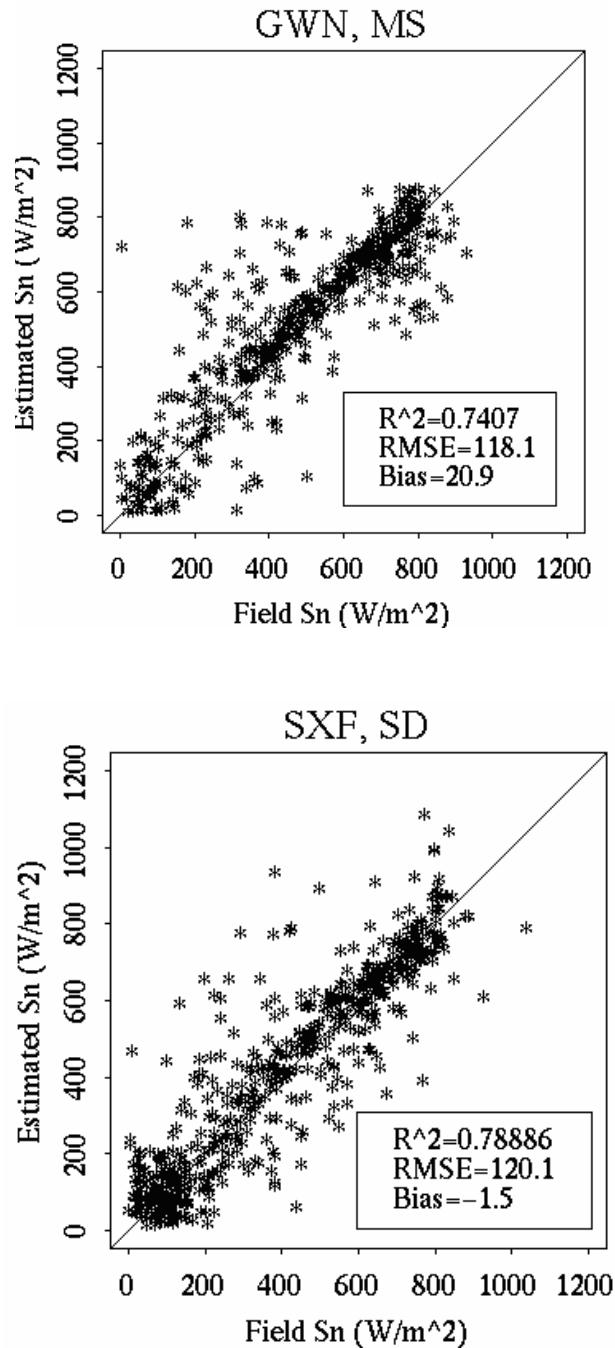


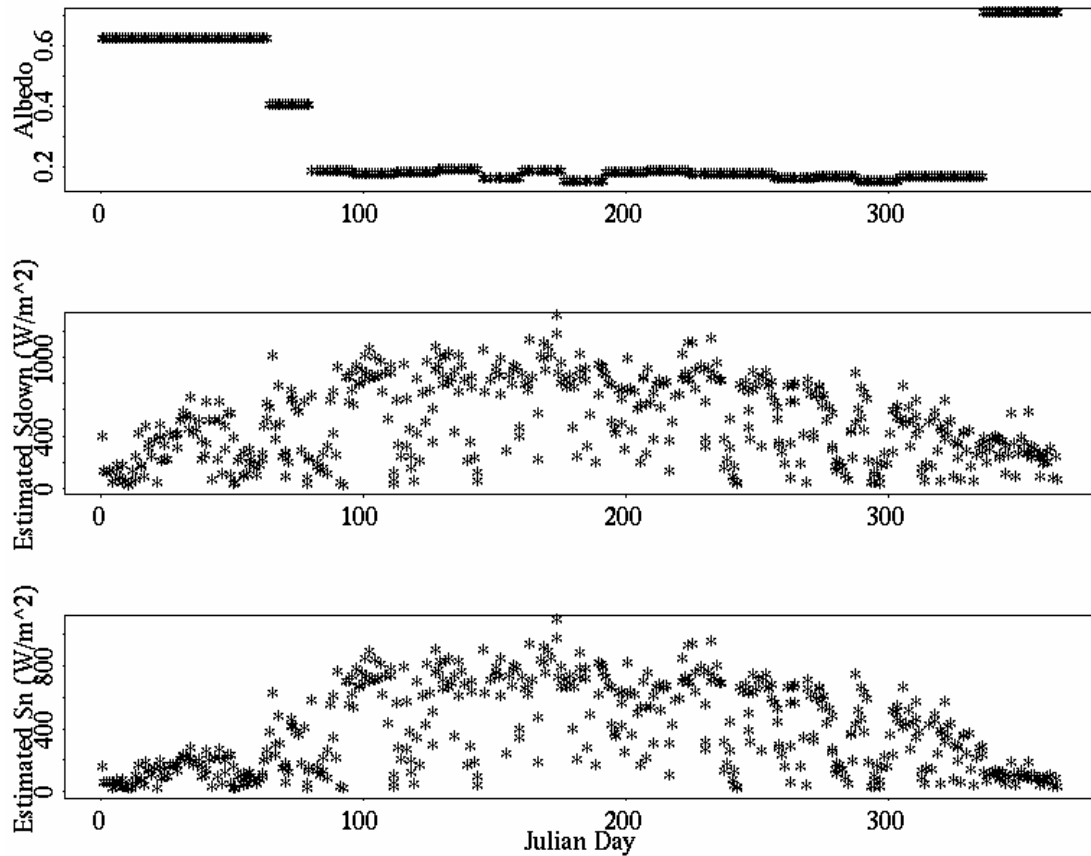
Table 2- 4 Validation of estimated shortwave net radiation using hybrid method (albedo-based estimation) at 1 km and time closest to satellite over pass

Sites	R ²	RMSE (Wm ⁻²)	Bias (Wm ⁻²)
BON	0.7810	116.1	12.5
TBL	0.6696	152.5	-80.9
GWN	0.7407	118.1	20.9
DRA	0.7791	84.8	9.5
FPK	0.7309	133.9	-41.9
PSU	0.7857	126.3	8.6
SXF	0.7886	120.1	-1.5
mean	0.7537	121.7	-10.4

Figure 2-9 shows extracted albedo, estimated S_{\downarrow} , and S_n over PSU sites.

Discontinuity in MODIS albedo is shown in extracted albedo. The MODIS albedo was not observed in the early days of year, therefore larger RMSEs in the albedo-based estimation are suspected due to the mismatch in temporal and spatial resolution. The same albedo values were used for the first 60 days due to a seasonal snow cover, and this reduced the estimated variation in S_n . Ground measured S_n extended up to 600 Wm⁻² during this period of time while albedo-based S_n estimates extended only to 260 Wm⁻². The same phenomenon was observed during the last 30 days of the year. Albedo-based S_n estimates only extended to 170 Wm⁻² while ground measurements extended to 470 Wm⁻². Temporal resolution difference and data gap in input data result in large RMSEs. This might indicate that errors in input data could affect the final results.

Figure 2- 9 Shortwave net radiation estimation using albedo-based estimation over PSU sites. Top: albedo values used in albedo-based shortwave net radiation estimation, middle: estimated shortwave downward radiation, and bottom: estimated shortwave net radiation using albedo-based estimation



2.4.3 Data aggregation using direct estimation

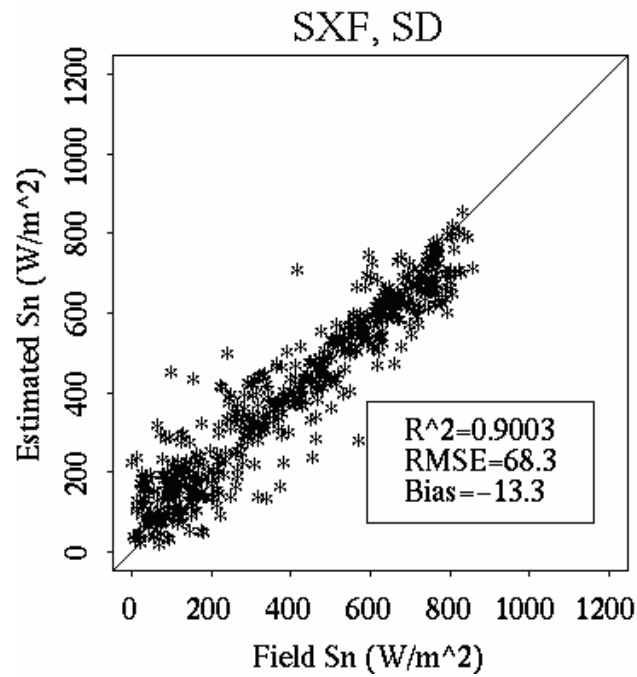
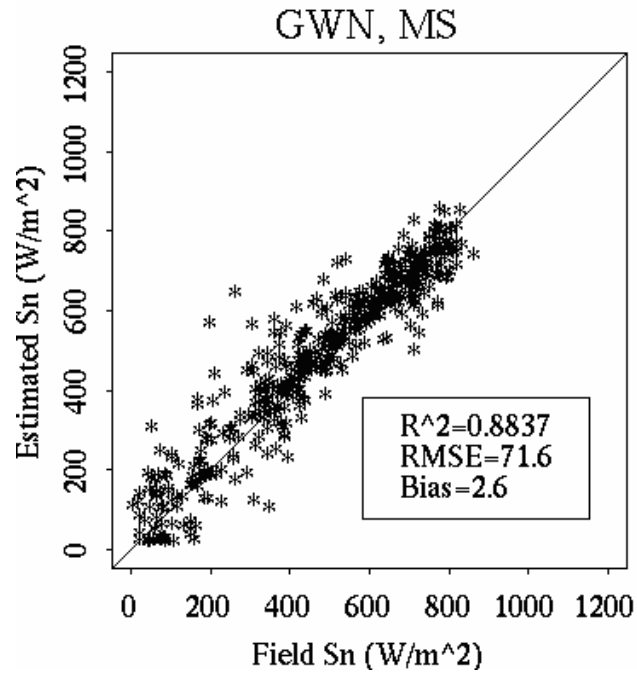
The heterogeneity effect due to optical depth variability and the horizontal transport effect of light moving between cloud columns (usually referred to as 3-D cloud effect) affects the accurate estimation of S_n . The 1-D radiative transfer models,

ignore the 3-D cloud effects, assuming that clouds are plane-parallel and homogeneous. 1-D models, therefore, are unable to accurately describe the radiation field at small scales (Barker and Davies, 1992; Cahalan et al., 1994; Loeb et al., 1998; Varnai, 2000). The hybrid algorithms do not account for the 3-D cloud effects; however, aggregation to a resolution of 9-km could mitigate the 3-D cloud effects. To reduce the large variance caused by broken cloud fields, ground measurements are averaged over a 30-minute window centered at satellite-overpass time. Figure 2-10 compares estimated and field measured S_n . Table 2-5 summarizes the statistical comparison. RMSEs are reduced to 68.1 – 99.9 Wm^{-2} by aggregating to a spatial resolution of 9-km and a 30-minute time window.

Table 2- 5 Validation of estimated shortwave net radiation using hybrid method (direct estimation) at 9 km and 30 minute time window

Sites	R²	RMSE (Wm^{-2})	Bias (Wm^{-2})
BON	0.8761	76.3	-5.5
TBL	0.8062	96.7	-40
GWN	0.8837	71.6	2.6
DRA	0.8469	68.1	-49
FPK	0.8686	79.9	-29.3
PSU	0.8165	99.9	23.7
SXF	0.9003	68.3	-13.3
mean	0.8569	80.1	-15.8

Figure 2- 10 Validation of estimated shortwave net radiation using hybrid method (direct estimation) at 9 km and 30 minute time window



2.5 Comparison with other products

Current products (GEWEX/SRB and ISCCP) and physically-based method is compared to ground measurement over the seven SURFRAD sites.

2.5.1 Comparison with GEWEX data

The data contain 3-hourly global fields of shortwave surface net radiation derived with the shortwave algorithm of the NASA World Climate Research Programme/Global Energy and Water-Cycle Experiment (WCRP/GEWEX) surface radiation budget project. The data were generated on a nested grid that contains 44016 cells. The grid has a resolution of 1 degree latitude globally, and longitudinal resolution ranging from 1 degree in the tropics and subtropics to 120 degrees at the poles (Stackhouse, 2004).

I extracted grid cells at the seven SURFRAD sites and compared them with ground measurements. Release 2.8 data were used and currently data from January to June in year 2005 are available. Figure 2-11 compares the estimated and surface measured shortwave net radiation. Table 2-6 provides a statistical comparison of the estimated and surface-measured S_n .

Figure 2- 11 Comparison of shortwave net radiation from GEWEX/SRB data from January to June 2005 for the SURFRAD sites

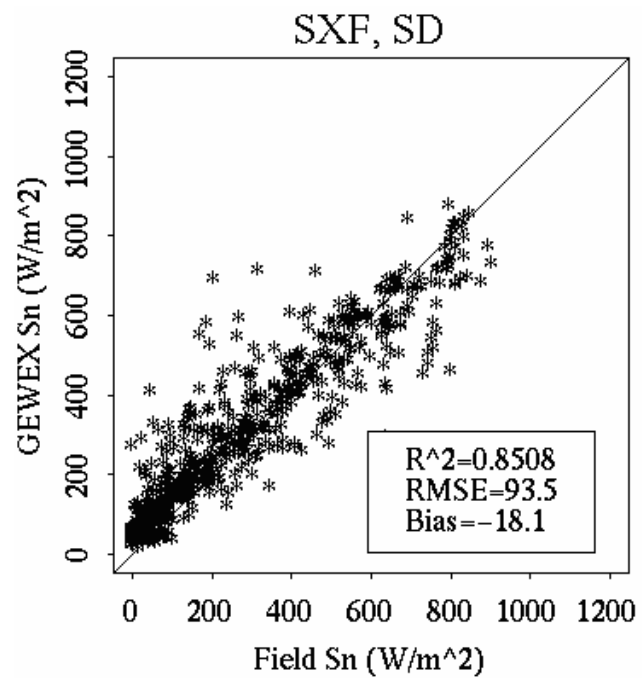
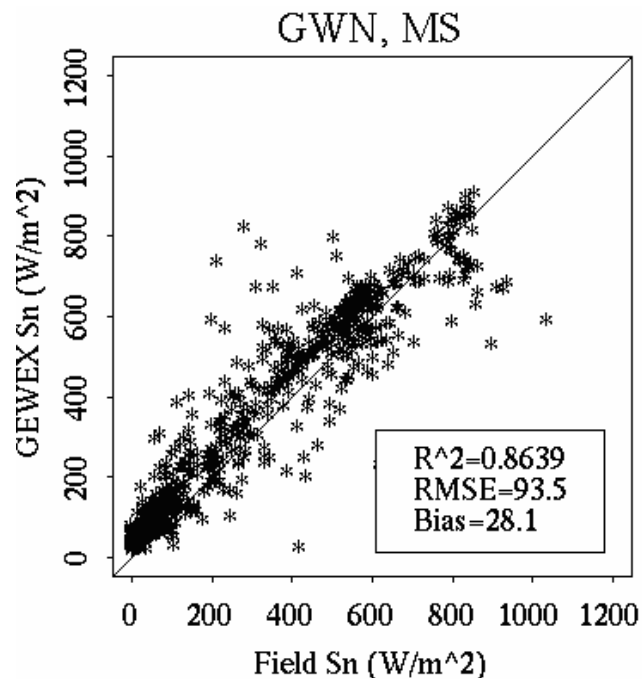


Table 2- 6 Comparison of shortwave net radiation from GEWEX/SRB data (1 degree resolution) from January to June 2005 for the seven SURFRAD sites

Sites	R ²	RMSE (Wm ⁻²)	Bias (Wm ⁻²)
BON	0.8489	96.1	37.3
TBL	0.6815	158.3	-23.6
GWN	0.8639	93.5	28.1
DRA	0.8278	118.5	29.7
FPK	0.8367	99.9	-5.9
PSU	0.7970	109.4	48.8
SXF	0.8508	93.5	18.1
mean	0.8152	109.9	18.9

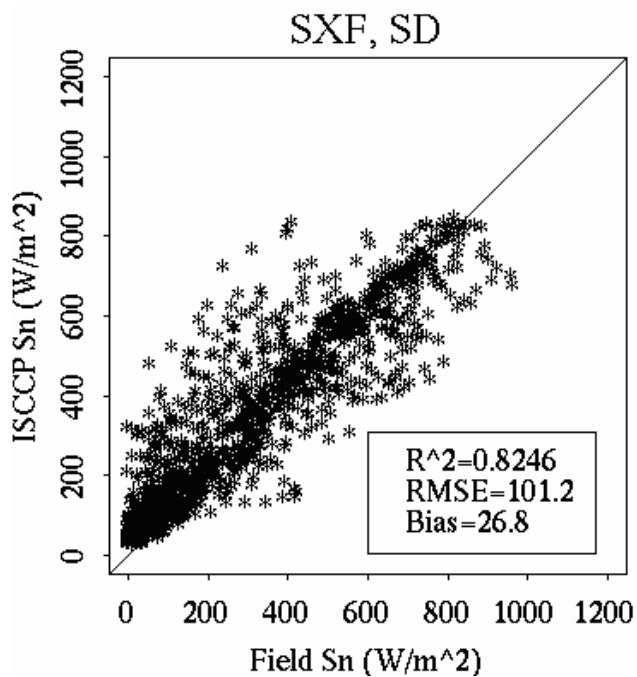
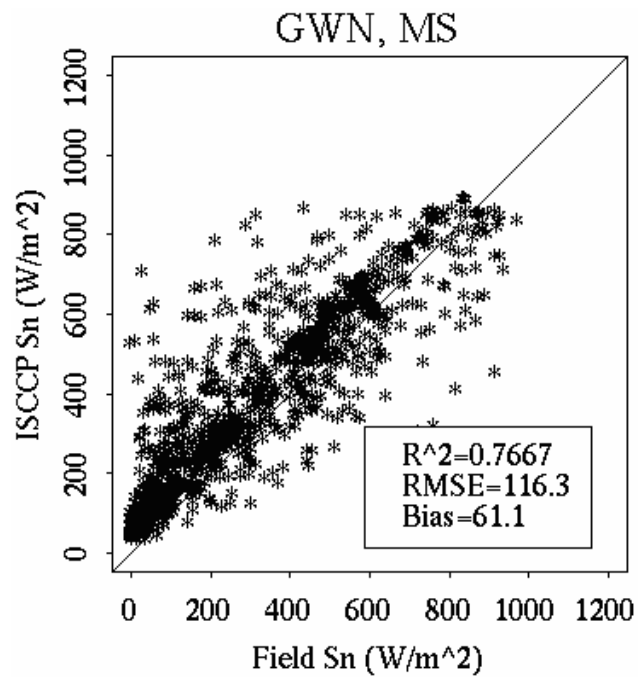
2.5.2 Comparison with ISCCP data

The ISCCP FD-SRF RadFlux dataset were used in this comparison. Reprocessed data from year 1983 to year 2004 are available on a 280 km equal-area grid (about 2.5 degrees) and a 3-hour temporal resolution (Zhang et al., 2004). Data from 2004 were extracted to provide a comparison of different spatial resolution products. Validation results are shown in Figure 2-12 and summarized in Table 2-7.

Table 2- 7 Comparison of shortwave net radiation from ISCCP data (2.5 degree resolution) 2004 for the seven SURFRAD sites

Sites	R ²	RMSE (Wm ⁻²)	Bias (Wm ⁻²)
BON	0.5887	148.7	41.0
TBL	0.7062	143.6	-10.0
GWN	0.7667	116.3	61.1
DRA	0.8778	92.4	-29.0
FPK	0.8568	93.0	12.3
PSU	0.7845	105.8	49.5
SXF	0.8246	101.2	26.8
mean	0.7722	114.4	21.7

Figure 2- 12 Comparison of shortwave net radiation from ISCCP data (2.5 degree resolution) 2004 for the SURFRAD sites



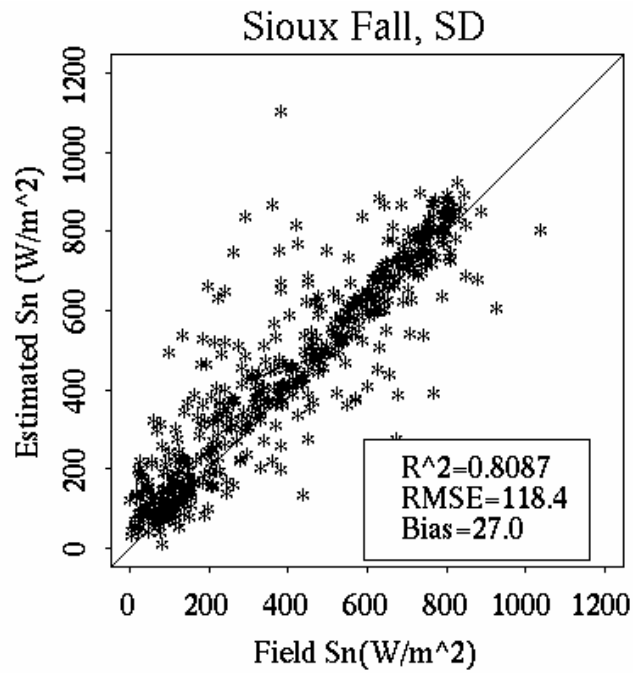
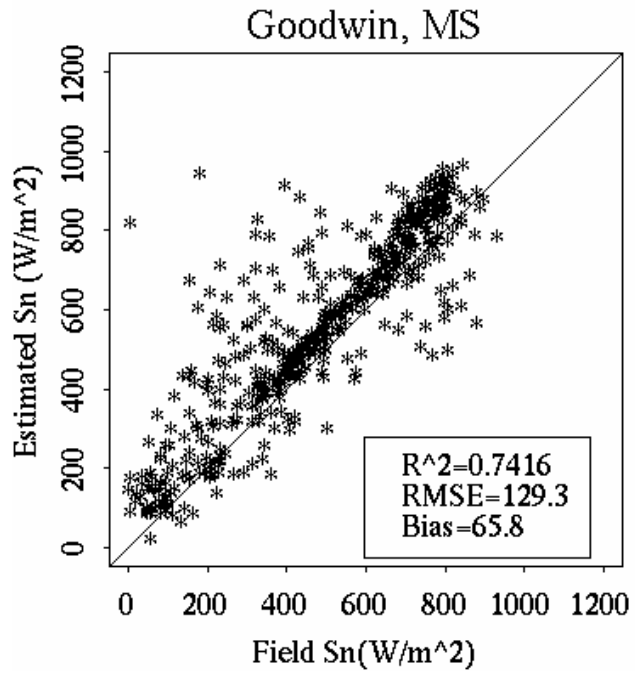
2.5.3 Comparison with a physically based method

Tang et al (2006) method was implemented in this study to examine how the physically-based method works in S_n estimation. Section 2.1 describes this method. The data used in implementation were MOD021KM, MOD03, and MOD05_L2 from 2005. Figure 2-13 compares S_n estimated with the physically-based method to S_n measured at the SURFRAD sites. A statistical comparison of the results is provided in Table 2-8. The physically-based method produces RMSEs of 103.8 – 153.7 Wm^{-2} and accuracy is less than hybrid method (direct estimation, average RMSE 93.8 Wm^{-2}).

Table 2- 8 Shortwave net radiation estimation validation for the seven SURFRAD sites using the physically-based method

Sites	R²	RMSE (Wm^{-2})	Bias (Wm^{-2})
BON	0.7252	113.3	40.74
TBL	0.6287	153.7	-5.33
GWN	0.7416	129.3	65.8
FPK	0.7241	136.5	11.5
DRA	0.7537	103.8	-1.8
PSU	0.7391	129.7	57.9
SXF	0.8087	118.4	27.0
mean	0.7316	126.4	28.0

Figure 2- 13 Validation results for physically-based method for shortwave net radiation estimation



2.6 Summary

A hybrid method to estimate shortwave net radiation (S_n) was developed in this study. This method does not require coarse resolution ancillary data; therefore, the spatial resolution of the original input data can be retained. The hybrid method estimates all-sky S_n was estimated at 1 km resolution with average RMSE of 93.8 Wm^{-2} . The average RMSE is reduced to 80.1 W m^{-2} when data were aggregated to a resolution of 9-km and ground measurements are averaged over a 30-minute time window.

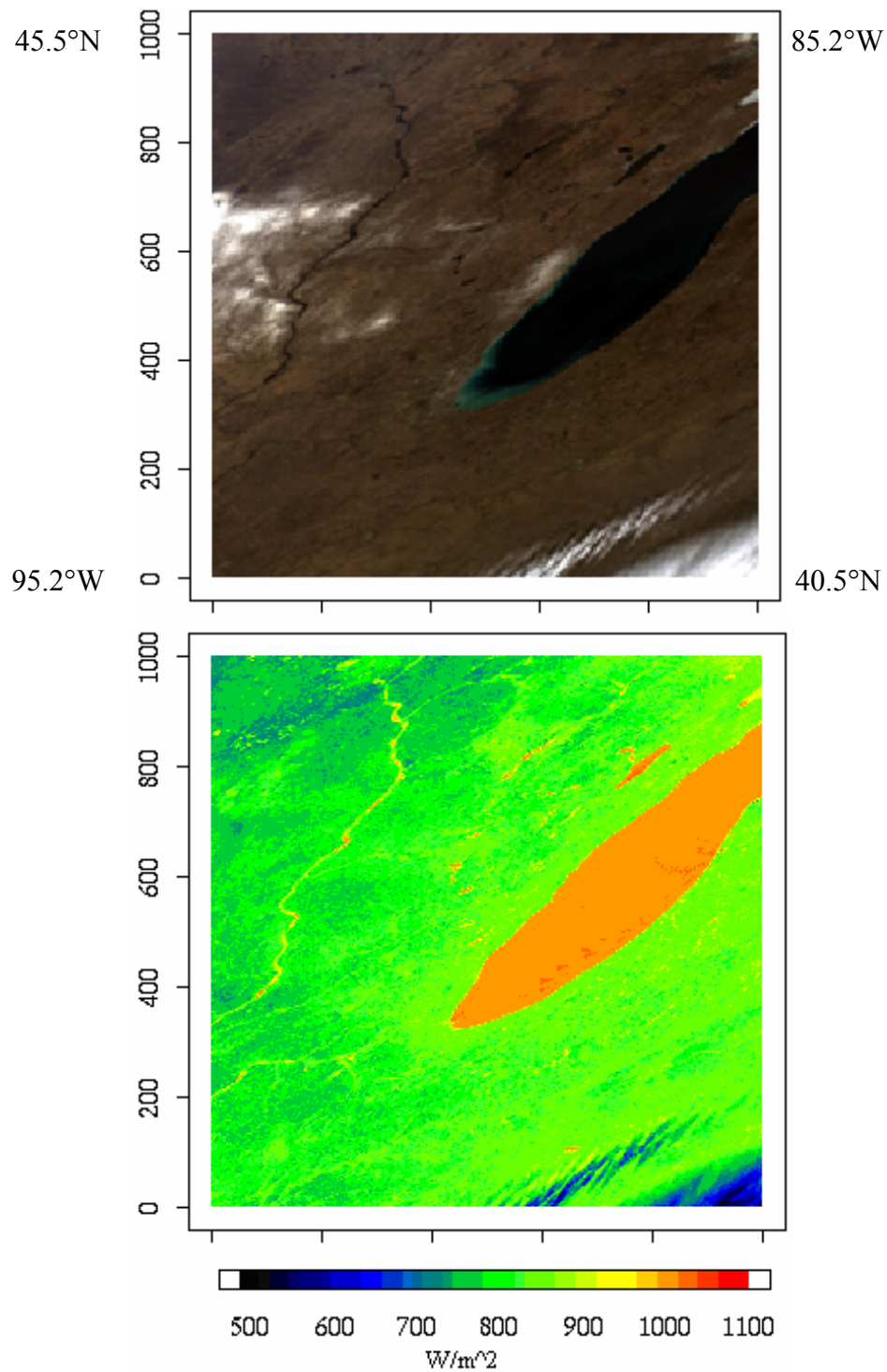
Estimated S_n using the hybrid method at 1-km resolution and GEWEX/SRB data from January to June in 2005 were compared. The validation results are provided in Table 2-8 with ISCCP data from 2004. The hybrid algorithm results at 1 km resolution have smaller errors than GEWEX/SRB (1 degree) or ISCCP (2.5 degree) data. The hybrid algorithm produces less RMSE and bias by 12% and 2% respectively compared to GEWEX/SRB data (half of a year's data are evaluated). Compared to ISCCP data, the RMSE and bias are less by 14% and 4% respectively (one year's data are evaluated). Estimated S_n using the hybrid method at 1-km resolution is in much better agreement with surface measurements than 1 degree and 2.5 degree data due to the improved scale matching. S_n products at less than 1 degree resolution are, however, not available currently, S_n estimated by hybrid method is recommended to use for finer resolution application. Estimated S_n using hybrid method will be used in the remainder of this study.

Implementing the new hybrid algorithm is very straightforward. Figure 2-14 shows a color composite of MODIS TOA reflectance data and direct-estimated S_n on day 99 in 2005 (band combination: band 1 in red, band 4 in green, and band 3 in blue).

Table 2– 9 Comparisons of hybrid method (1 km), GEWEX/SRB (1 degree), and ISCCP data (2.5 degree). RMSE as a percentage of mean observation is presented in parenthesis. RMSE and Bias are in unit of Wm^{-2}

Sites	Hybrid (Jan. – Jun. 2005)			GEWEX (Jan. – Jun. 2005)			ISCCP (2004)		
	R ²	RMSE(%)	Bias(%)	R ²	RMSE(%)	Bias(%)	R ²	RMSE(%)	Bias(%)
BON	0.8267	95.0(23)	2.7(1)	0.8489	96.1(29)	37.3(11)	0.5887	148.7(47)	41.0(12)
TBL	0.8038	103.9(21)	-54(11)	0.6815	158.3(48)	-23.6(7)	0.7062	143.6(44)	-10.0(3)
GWN	0.8562	89.8(19)	1.2(0)	0.8639	93.5(26)	28.1(8)	0.7667	116.3(32)	61.1(17)
DRA	0.8522	71.7(13)	-61(11)	0.8278	118.5(28)	29.7(7)	0.8778	92.4(23)	-29.0(7)
FPK	0.7794	102.2(27)	-20(5)	0.8367	99.9(36)	-5.9(2)	0.8568	93.0(36)	12.3(5)
PSU	0.8117	108.0(28)	19.0(5)	0.7970	109.4(36)	48.8(16)	0.7845	105.8(37)	49.5(17)
SXF	0.8360	88.6(23)	-9.6(2)	0.8508	93.5(31)	18.1(6)	0.8246	101.2(33)	26.8(9)
mean	0.8237	94.1(22)	-17.6(5)	0.8152	109.9(34)	18.9(8)	0.7722	114.4(36)	21.7(10)

Figure 2- 14 Color composite of MODIS TOA reflectance over southern Lake Michigan, acquired on day 99 in 2005 and estimated shortwave net radiation by direct estimation. Units are in Wm^{-2}



Chapter 3: Estimating Cloudy-sky Net Radiation

Surface all-wave net radiation (R_n) controls the input of latent and sensible heat flux into the atmosphere over the Earth's surface, therefore, R_n is a factor in determining long-term weather and climate. R_n is also a key parameter in computing reference evapotranspiration and is a driving force in many other physical and biological processes.

R_n is the sum of downward and upward components in shortwave and longwave radiation as shown by equation 1-1. Measured R_n is available only from well-equipped weather stations; therefore, R_n measurements of high temporal and spatial resolution are scarce (Alados et al., 2003; Allen, 1996). Hence, calculated values of R_n are commonly used instead of measured R_n (Samani et al., 2007).

3.1 Background

When meteorological data are used, linear regression, multivariate regression, and physically-based models are applied (Kjaersgaard et al., 2007). Linear regression estimation of R_n uses shortwave net radiation (Alados et al., 2003; Kaminsky and Dubayah, 1997); multivariate regression estimation of R_n uses mean daily air temperature, Earth-Sun distance, and downward solar radiation (Irmak et al., 2003a). Physically-based models estimate R_n by calculating the individual terms in equation 1-1 separately. S_n is calculated by $S\downarrow(1 - \text{albedo})$ and longwave net radiation (L_n) estimation procedures are often based on the theoretical Stefan-Boltzmann Law that

states that the energy radiated from the surface of a black body is proportional to its emissivity and the fourth power of its temperature. Equation 3-1 was suggested for L_n calculation (Hansen, 2000):

$$L_n = (\varepsilon_s L_c \downarrow - L \uparrow)(c_1 \frac{S \downarrow}{S_c \downarrow} + c_2) \quad (3-1)$$

where ε_s is surface emissivity, $L_c \downarrow$ is clear-sky downward longwave radiation, $S_c \downarrow$ is clear-sky downward shortwave radiation, and c_1 and c_2 are empirical coefficients that require local calibration. The calibration coefficients require local calibration and, therefore, are only valid for a spatially limited area or region.

When satellite data are used, Jacobs et al. (2004) calculated L_n with Equation 3-2:

$$L_n = (1 - \varepsilon_s)(L_c \downarrow + (1 - \varepsilon_a)C\sigma T_c^4) - \varepsilon_s \sigma T_s^4 \quad (3-2)$$

where ε_s is surface emissivity, $L_c \downarrow$ is clear-sky downward longwave radiation, ε_a is atmospheric emissivity, T_c is cloud temperature (cloud-base temperature), C is the effective cloud fraction, σ is Stefan-Boltzman constant, and T_s is surface temperature. Satellite estimation of R_n has the advantage of global spatial coverage; however, the errors associated with input parameters can affect the accuracy of results. Errors at each step in the estimation potentially cancel or reinforce each other. Also, the resolution of raw data is not retained when satellite-based cloud information is used (Garatuza-Payan et al., 2001; Jacobs et al., 2004; Stewart et al., 1999). Cloud -top

temperature, instead of cloud-base temperature, is used in Equation 3-2 because cloud-base temperature is hard to be retrieved using satellite data.

A high-resolution method of estimating cloudy-sky R_n is necessary to support recent ecosystem simulations. The method of estimating R_n without using retrieved cloud properties was explored because of uncertainties in retrieval of cloud properties from satellite data. The goal is to define relationship between S_n and R_n under cloudy-sky by considering surface characteristics, because energy exchange between the Earth and atmosphere is controlled by R_n and R_n is closely related to surface characteristics.

3.2 Cloudy-sky net radiation estimation method

Although there are many applications for R_n , the R_n data are rarely available due to the technical and economical limitations inherent in direct measurements (Samani et al., 2007). Estimating surface longwave net radiation (L_n) from satellite data is especially difficult under cloudy-sky conditions; therefore, empirical formulae for estimating cloudy-sky R_n would be extremely helpful to the user community. The proposed approach estimates R_n (0.2 – 100 μm) using S_n (0.2 – 4.0 μm) and vegetation indices and is based on surface S_n measurements. The FLUXNET sites used to develop the formulae to estimate cloudy-sky R_n are listed in Table 3-1. FLUXNET is a global network of micrometeorological tower sites that measure the exchange of carbon dioxide, water vapor, and energy between the terrestrial ecosystem and

atmosphere (Baldocchi et al., 2001). Five or more years of data were collected from 13 FLUXNET sites with different Plant Functional Types (PFT).

Table 3- 1 Location and plant functional types (PFT) of FLUXNET sites used in surface all-wave net radiation study

Station	Latitude	Longitude	PFT
Audubon	31.60	-110.51	Grass
Blackhills	44.16	-103.65	Evergreen Needleleaf Trees
Bondville	40.01	-88.29	Broadleaf Crop
Fort Peck	48.31	-105.10	Grass
Goodwin	34.25	-89.97	Broadleaf Crop
Lost Creek	46.08	-89.98	Deciduous Broadleaf Trees
Mead (irrigated)	41.10	-96.29	Broadleaf Crop
Mead (rainfed)	41.10	-96.44	Broadleaf Crop
MMSF	39.32	-86.41	Deciduous Broadleaf Trees
Niwot	40.03	-105.55	Evergreen Needleleaf Trees
Walnut River	31.52	-96.86	Grass
Willow Creek	45.81	-90.08	Deciduous Broadleaf Trees
Wind River	45.82	-121.95	Evergreen Needleleaf Trees

3.2.1 Identifying cloudy-sky conditions

The temporal window of three ground measurements in shortwave downward radiation (S_{\downarrow}) is taken during the day (x_1 , x_2 , and x_3) and assumed to have a linear relationship under clear-sky condition (Figure 3-1). Cloudy-skies are assumed if the center S_{\downarrow} datum (x_2) satisfies the following equation:

$$x_2 < \frac{x_1 + x_3}{2} - \sigma \quad (3-3)$$

where σ is the standard deviation. Setting a threshold in S_{\downarrow} to identify cloudy-sky conditions eliminated cloudy-sky data in winter. Extracted cloudy-sky data were

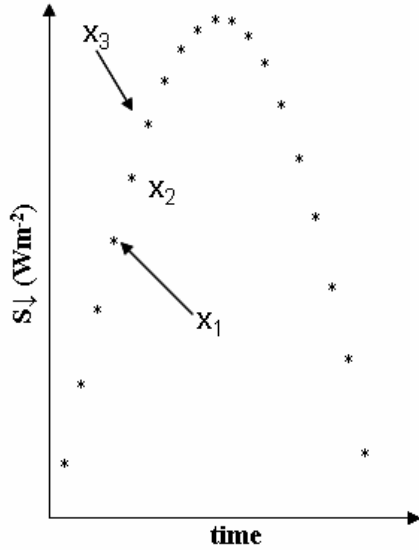


Figure 3- 1 Variation in clear-sky shortwave downward radiation over the course of one day

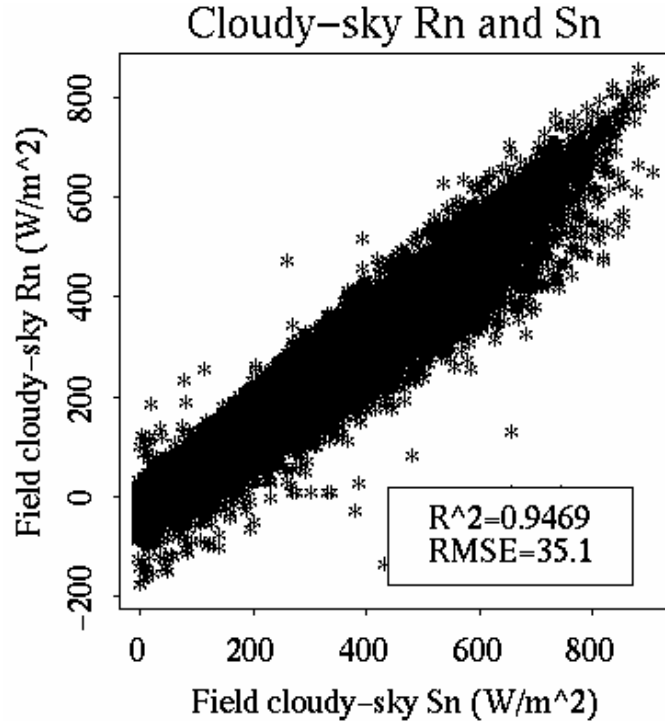
confirmed by daily weather database (<http://www.wunderground.com/>) if station records are available.

After extracting cloudy-sky data, the relationship between R_n and S_n is established using Equation 3-4. Figure 3-2 shows this relationship.

$$R_n = 20.1898 + 0.8347 \cdot S_n \quad (3-4)$$

It shows that they are related (R^2 is 0.9469) in RMSE 35.6 Wm^{-2} .

Figure 3- 2 Field cloudy-sky all-wave net radiation and shortwave net radiation



3.2.2 Multivariate regression analysis

Net radiation controls the total energy exchange between the atmosphere and the Earth's surface and it is closely related to surface characteristics. PFT is used to categorize the surface. PFT can be extracted from MODIS land cover classification products (MOD12Q1). Table 3-2 lists the PFT types from MOD12Q1. After grouping cloudy-sky ground measurements into PFTs, the Enhanced Vegetation Index (EVI) is used to describe surface vegetation status. EVI is extracted from MODIS vegetation indices products (MOD13A2). Two vegetation indices are included: One is the standard normalized difference vegetation index (NDVI), which is referred to as the "continuity index" to the existing National Oceanic and Atmospheric Administration

(NOAA)-Advanced Very High Resolution Radiometer (AVHRR) derived NDVI. The other is an EVI with improved sensitivity in high biomass regions and improved vegetation monitoring through a de-coupling of the canopy background signal and a reduction in atmosphere influences. Both indices were applied, and EVI produced better results. EVI and S_n are used to estimate R_n with equation 3-5.

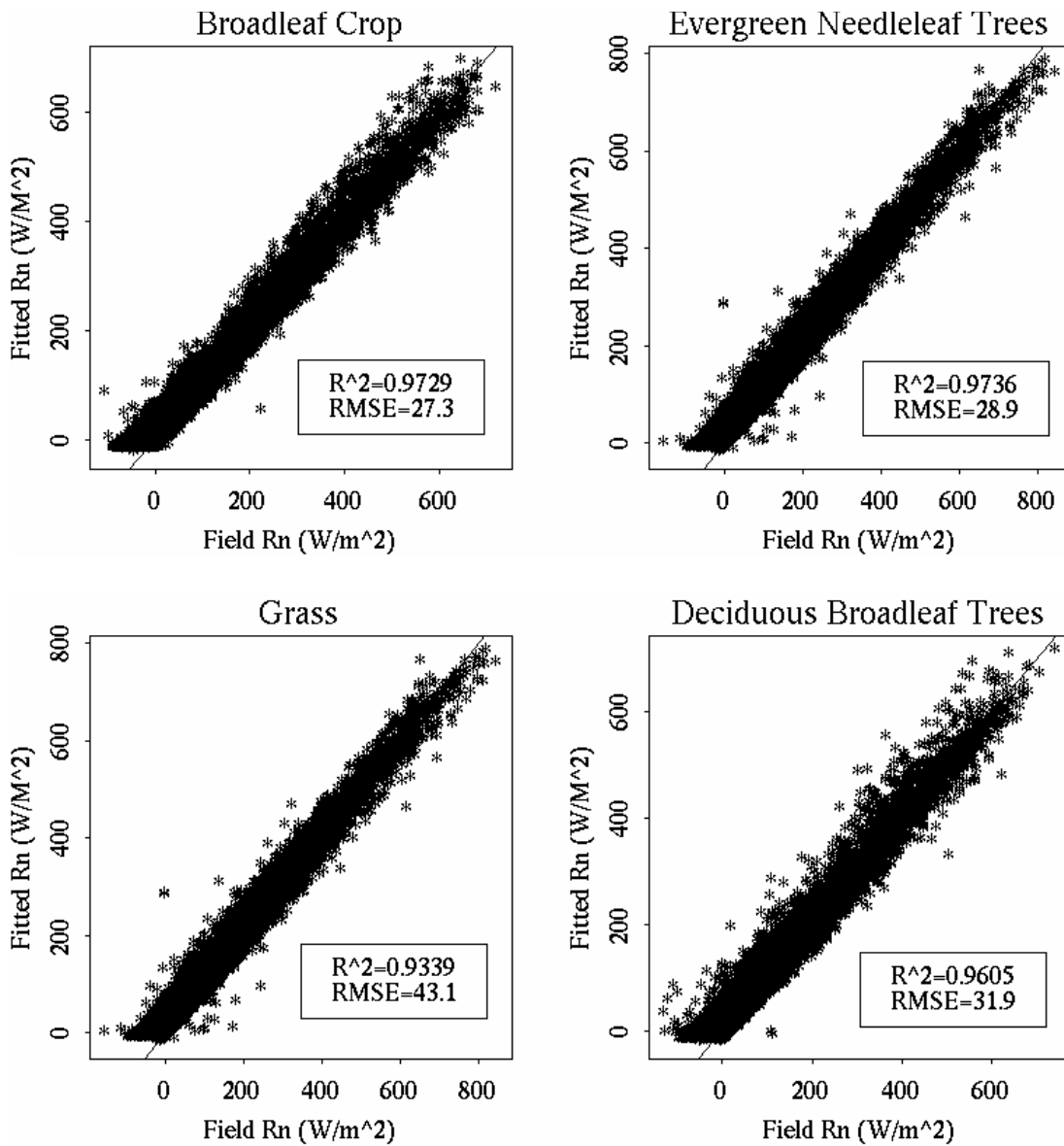
$$R_n = a_0 + a_1EVI + a_2S_n + a_3S_n \cdot EVI \quad (3-5)$$

R_n estimation is improved when surface characteristics are considered except for grass surfaces (Table 3-2). Surface characterization does not appreciably improve accuracy for grass because EVI in grass is usually low and less improvement by surface characteristics is observed. In addition, exposed soil and dead grass could increase the outgoing thermal radiation and decrease accuracy (Fritschen and Ping, 1992).

Table 3- 2 Regression coefficients used to estimate cloudy-sky all-wave net radiation

PFT	a_0	a_1	a_2	a_3	R^2	RMSE
Broadleaf crop	-18.57	8.05	0.76	0.19	0.9729	27.4
Evergreen needleleaf	-11.84	-6.19	0.86	0.03	0.9736	28.9
Grass	-35.46	36.39	0.66	0.46	0.9339	43.1
Deciduous broadleaf	-14.40	-15.32	0.74	0.24	0.9605	31.9

Figure 3- 3 Cloudy-sky all-wave net radiation fitting dependant on plant functional types



3.2 Validation results

Two SURFRAD sites are classified broadleaf crop: Bondville (IL) and Penn State (PA). Coefficients from broadleaf crop in Table 3-2 are used in cloudy-sky R_n

estimation by Equation 3-5. The described procedures were implemented and validation results are shown in Figure 3-4.

CERES/ARM Validation Experiment (CAVE) Clouds & Radiative Swath (CRS) footprint validation under overcast for Bondville and Penn state sites (Table 3-3, <http://snowdog.larc.nasa.gov/cave/pages/valplot.html>) is provided because I failed to find any papers that reported errors for cloudy-sky R_n explicitly. Table 3-3 does not provide cloudy-sky all-wave net radiation directly, and it is too complex to know how error terms related in shortwave and longwave work in all-wave net radiation. Table 3-3 illustrates basic concepts of radiation estimation under cloudy-sky conditions. Average RMSEs of 107.6 and 49.3 Wm^{-2} are shown in S_{\downarrow} and S_{\uparrow} , and 18.2 and 17.7 Wm^{-2} in longwave downward radiation and in longwave upward radiation respectively.

Figure 3- 4 Validation of all-wave net radiation estimation under cloudy-sky for broadleaf crop plant functional type

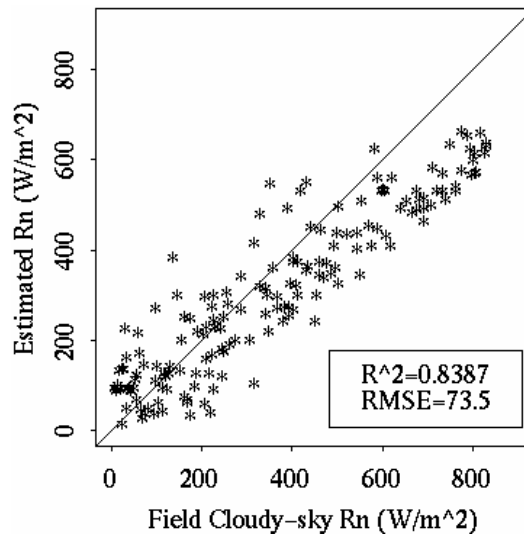


Table 3- 3 Errors related to surface radiation budget components estimation under cloudy-sky: (a) Bondville, IL and (b) Penn State, PA

(a) Bondville, IL

Overcast MODIS

	Obs Mean	N	Bias CRS-Obs	Std Dev	RMS	Mod Frc All-Clr	Forcing All-CNA
LW Dn Sfc	348.2	112	-6.4	16.9	18.0	46.2	0.6
LW Up Sfc	366.2	112	8.7	20.5	22.2	-----	-----
SW Dn Sfc	205.3	57	20.2	103.7	104.7	-431.0	-10.2
SW Up Sfc	60.0	55	-25.9	42.0	49.0	-----	-----
LW Up TOA	181.0	112	2.9	9.1	9.6	-67.7	-0.1
SW Up TOA	489.3	57	14.3	17.4	22.4	340.5	0.7

(b) Penn State, PA

Overcast MODIS

	Obs Mean	N	Bias CRS-Obs	Std Dev	RMS	Mod Frc All-Clr	Forcing All-CNA
LW Dn Sfc	340.1	126	-8.3	16.4	18.3	49.0	0.5
LW Up Sfc	360.9	126	2.4	12.9	13.1	-----	-----
SW Dn Sfc	239.1	69	2.0	111.2	110.4	-463.7	-8.6
SW Up Sfc	62.3	66	-25.4	42.8	49.5	-----	-----
LW Up TOA	184.1	126	3.4	9.3	9.9	-61.0	-0.1
SW Up TOA	508.4	69	18.2	25.2	31.0	351.5	0.3

Chapter 4: Daily Net Radiation Estimation

Studies have shown that integrated S_n is required in land surface models at daily temporal resolution. Studies have used air temperature, other meteorological data sets, or simply substituted one from the closest station in estimating daily integrated S_n (Fletcher and Moot, 2007; Hunt et al., 1998; Rivington et al., 2005; Wu et al., 2007). Daily integrated S_n is major input parameter in land surface models, therefore, errors in estimation of daily integrated S_n can lead significant distortion of model output. 10 to 30% of errors in crop yield due to the errors in integrated S_n were reported (Trnka et al., 2007).

Two methods exist to estimate daily solar irradiance: 1) estimation with meteorological datasets (Friend, 1998; Winslow et al., 2001), and 2) estimation with satellite data (Pinker and Laszlo, 1992; Gu and Smith, 1997; Lefevre et al., 2007). Limited spatial coverage is a major drawback when meteorological data sets are used. Daily integrated net radiation using satellite data is not currently reported and monthly average S_n is used in studies. Data averages, however, eliminate the exact sequence of cold-or-warm, wet-or-dry days that is an important factor in processes such as vegetation net primary production (Hunt et al., 1991). Therefore, this is the first effort to estimate daily integrated S_n from satellite data and a method is described in this section.

4.1 Estimation algorithm

The following equations are used in current method to estimate daily integrated S_n . If a solar radiation measurement is not available, it can be estimated from extraterrestrial radiation (Samani et al., 2007).

$$\text{Daily SRB} = K_r (T_{\max} - T_{\min})^{0.5} R_a \quad (4-1)$$

where T_{\max} and T_{\min} are daily maximum and minimum air temperature ($^{\circ}\text{C}$), R_a is extraterrestrial radiation on daily basis and is calculated by procedures developed by Duffie and Beckman (1980, 1991) as

$$R_a = \frac{1440}{\pi} G d_r [\omega_s \sin(\phi) \sin(\delta) + \cos(\phi) \cos(\delta) \sin(\omega_s)] \quad (4-2)$$

where G is the solar constant ($0.082 \text{ MJm}^2/\text{min}$), d_r is the inverse relative distance from the Earth to the Sun, ϕ is latitude, and ω_s is the sunset hour angle (rad).

K_r is suggested by Allen (1995) to be:

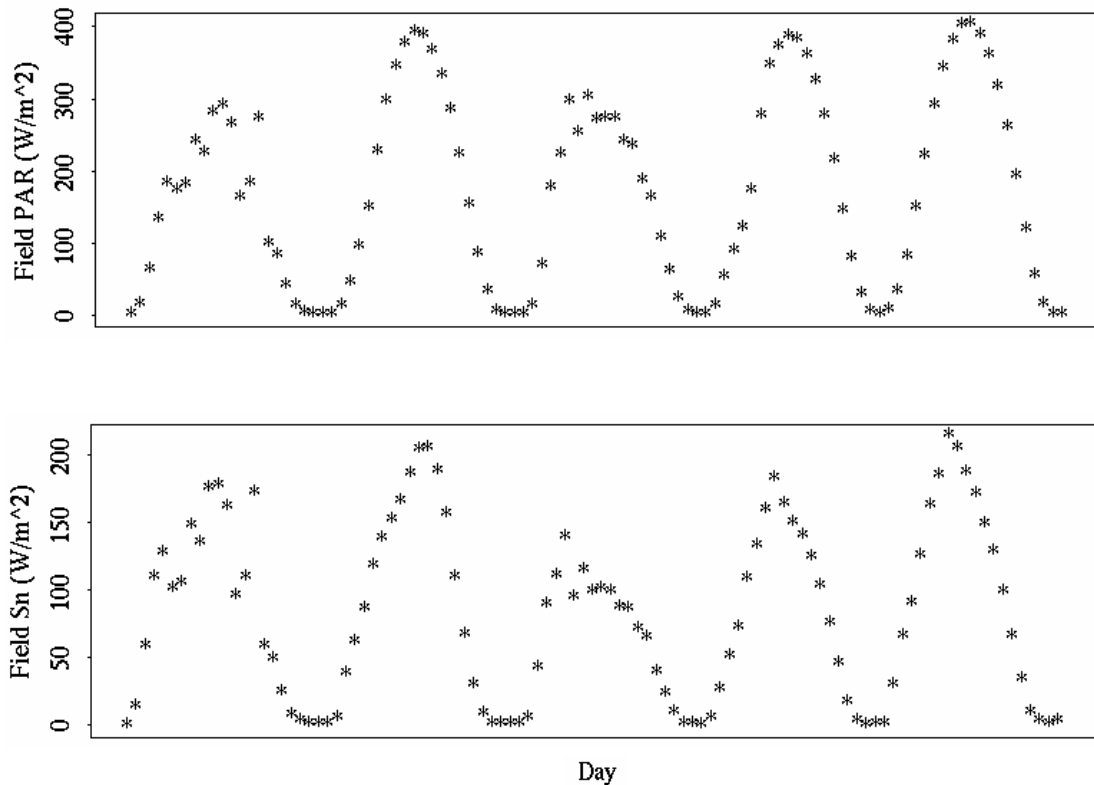
$$K_r = K_{ra} \left(\frac{P}{P_0}\right)^{0.5} \quad (4-3)$$

where P is the mean atmospheric pressure at the site (kPa), P_0 is mean atmospheric pressure at sea level, and K_{ra} is an empirical coefficient equal to 0.17 for interior

continental regions and 0.2 for coastal regions. When the above equations are applied to estimate daily integrated S_n , RMSEs of 3.42 – 5.88 MJm⁻² are reported.

Method for calculating daily-integrated S_n uses instantaneous S_n data as the input with the assumption of sinusoidal curve behavior during the daytime. This is called ‘adjusted sinusoidal interpolation method’ (Wang et al., 2008a). This method is applied to calculate daily integrated photosynthetically active radiation (PAR). The behavior of S_n is similar to that of PAR as shown in Figure 4-1, so adjusted sinusoidal interpolation is applied to calculate daily integrated S_n .

Figure 4- 1 Variation in ground measurements of photosynthetically active radiation (PAR) and shortwave net radiation (S_n) in Fort Peck, MT over the course of five days



Given one instantaneous S_n estimation at satellite overpass time ($T_{overpass}$), the instantaneous S_n value at any daytime t can be interpolated as:

$$Inst S_n = InstS_n(T_{overpass}) \frac{\sin \frac{(t - T_{sunrise})\pi}{T_{sunset} - T_{sunrise}}}{\sin \frac{(T_{overpass} - T_{sunrise})\pi}{T_{sunset} - T_{sunrise}}} \quad (4-4)$$

where π is the Archimedes' constant and $T_{sunrise}$ and T_{sunset} is the time of local sunrise and sunset at the location. If there are two observations at T_1 and T_2 , the S_n distribution functions derived from the two observations using Equation 4-4 are $InstS_nT_1(t)$ and $InstS_nT_2(t)$ respectively. From sunrise to T_1 , the S_n function is expressed as $InstSnT_1(t)$, and from T_2 to sunset, the S_n function is $InstSnT_2(t)$. Linear interpolation of the two sinusoidally interpolated values is used to calculate S_n between T_1 and T_2 using Equation 4-5:

$$Inst Sn(t) = \frac{T_2 - t}{T_2 - T_1} Inst Sn_{T_1}(t) + \frac{t - T_1}{T_2 - T_1} Inst Sn_{T_2}(t) \quad (4-5)$$

Once the instantaneous S_n function is known, daily-integrated S_n is calculated by using Equation 4-6.

$$Daily S_n = \int_{T_{sunrise}}^{T_{sunset}} Inst S_n(t) dt \quad (4-6)$$

If N observations are available ($T_1 \dots T_N$), Equation 4-5 is inserted in Equation 4-6:

$$\begin{aligned}
DailySn = & \int_{T_{sunrise}}^{T_1} Inst Sn_{T_1}(t)dt + \sum_{i=1}^{N-1} \int_{T_i}^{T_{i+1}} \left(\frac{T_{i+1} - t}{T_{i+1} - T_i} Inst Sn_{T_i}(t) + \frac{t - T_i}{T_{i+1} - T_i} Inst Sn_{T_{i+1}}(t) \right) dt \\
& + \int_{T_N}^{T_{sunset}} Inst Sn_{T_N}(t)dt
\end{aligned} \tag{4-7}$$

4.2 Validation

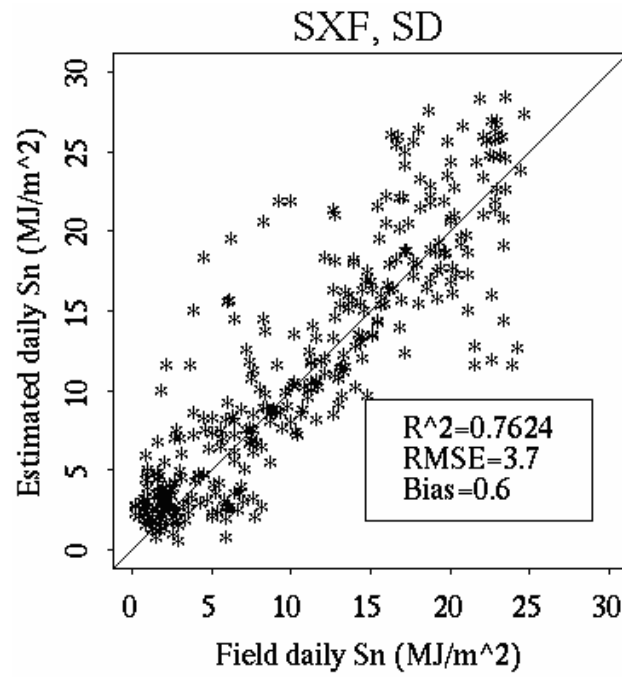
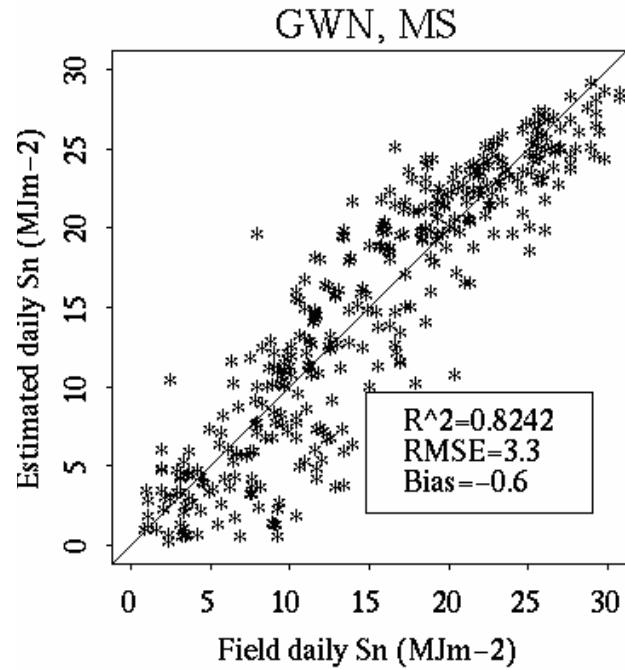
Estimated daily integrated shortwave net radiation (S_n) based on the method described above is compared with measurements from SURFRAD sites. The unit of instantaneous S_n is Watt per square meters and a time unit is added when S_n is integrated. Watts are converted to Joules per second, which changes the unit of integrated S_n to Joules per square meter. The numbers in Table 4-1 are in mega Joules per square meter. The results are also shown in Figure 4-2.

SURFRAD sites have a three-minute temporal resolution and there are three instantaneous S_n s maximally per day. Inconsistency in temporal resolution as well as spatial resolution causes these errors. The results show RMSEs of 2.8 – 4.0 MJm⁻²,

Table 4- 1 Validation of daily integrated shortwave net radiation, in Joules per square meter, at seven SURFRAD sites

Sites	R²	RMSE	Bias
BON	0.8773	2.8	1.3
TBL	0.7560	3.8	0.4
GWN	0.8242	3.3	-0.6
FPK	0.8100	3.5	-0.4
DRA	0.7366	3.4	-0.5
PSU	0.7809	4.0	1.3
SXF	0.7624	3.7	0.6
mean	0.7925	3.5	0.3

Figure 4- 2 Validation of daily integrated shortwave net radiation at seven SURFRAD sites



which are better than existing method ($3.42 - 5.88 \text{ MJm}^{-2}$). As shown in Equation 4-7, the more observation, the better agreement to surface measurements are expected. Therefore, the use of geostationary satellite data is recommended.

Chapter 5: Conclusions and future research

5.1 Estimating shortwave net radiation using MODIS data

A hybrid method has been developed to estimate instantaneous shortwave net radiation (S_n). The hybrid method, composed of a physical part and a statistical part, estimates shortwave net radiation without separating cloudy- or clear-sky conditions. The hybrid method estimates all-sky condition S_n and does not require ancillary data that typically have different spatial and spectral resolution; therefore, the spatial resolution of raw input data can be retained.

Two approaches are attempted in the hybrid method: 1) direct estimation, and 2) albedo-based estimation. The direct estimation method more accurately estimates surface-measured data. The standard MODIS albedo product were used in albedo-based method and inconsistency in temporal resolution between estimated downward radiation (S_{\downarrow}) and albedo product is suspected as a major source of error. Estimated S_n by direct estimation is used for cloudy-sky all-wave net radiation (R_n) estimation and daily integrated S_n .

Estimated S_n using the hybrid method at 1-km resolution is in better agreement with surface measurements than pre-existing products like 1 degree resolution GEWEX/SRB and 2.5 degree ISCCP dataset due to the improved scale matching. The hybrid algorithm produces a lower RMSE and bias by 12% and 2% respectively compared to GEWEX/SRB data and by 14% and 4% compared to ISCCP data sets.

Clearly, the spatial resolution of the remotely sensed data is crucial for discriminating surface net radiation for the different landscapes with significant variability in vegetation cover, type/architecture, and moisture. S_n at finer resolution can help avoiding significant errors due to application of a land surface model to a mixed pixel containing large contrast in surface. (Kustas and Norman, 2000; Moran et al., 1997).

5.2 Estimating cloudy-sky all-wave net radiation

All-wave net radiation (R_n) is the sum of shortwave net radiation (S_n) and longwave net radiation (L_n). Cloudy-sky conditions make estimating longwave net radiation from satellite data difficult. Therefore, cloudy-sky R_n estimation method from S_n and surface characteristics has been developed. This is the first effort to estimate cloudy-sky R_n by using vegetation type and status and S_n . Surface characteristics are considered by plant functional type and enhanced vegetation index from MODIS land cover type and vegetation indices product. The fitting is improved when surface characteristics are considered, and validation indicates that this method of estimating cloudy-sky R_n has a RMSE of 73.5Wm^{-2} . Comparison with other methods is difficult because no paper reported errors for cloudy-sky R_n explicitly.

5.3 Estimating daily integrated shortwave net radiation using MODIS data

This study describes a method of estimating daily integrated shortwave net radiation (S_n). The adjusted sinusoidal interpolation, used to estimate daily integrated photosynthetically active radiation (PAR), is adapted to estimate daily integrated S_n because S_n variation, over the course of a day, is similar to PAR variation. This is the first effort to estimate daily integrated S_n at a 1 km spatial resolution from MODIS data. Validation shows larger errors compared to instantaneous S_n estimation due to differences in spatial and sampling resolution between satellite data and SURFRAD sites. However, the validation results indicate an average RMSE of 3.5 MJWm⁻² that is comparable to other method. Another advantage of the suggested method is that it has greater spatial coverage compared to meteorological data.

All products estimated by method described in this study have a 1 km spatial resolution and comparable accuracy to pre-existing methods. These high resolution products are expected to support recent high resolution simulations in numerical weather and ecosystem models. The spatial resolution of the remotely sensed data is crucial for discriminating SRB for the different land cover types. Townshend and Justice (1988) degraded Land Remote Sensing Satellite (Landsat) imagery collected over a variety of landscapes to proposed pixel resolutions (250 m to 4 km) of the MODIS and show that for accurate assessment of land cover changes (which is related to S_n), a pixel resolution of 500 m or less is necessary (Townshend and Justice, 1988).

In addition, up-scaling from ground point measurements to the MODIS resolutions (1 km) using finer-resolution remotely sensed data is suggested because ground point

measurements may not be sufficient to validate the estimated measurements at MODIS resolutions even if surface is large and homogeneous or sufficient number of point measurements can be made during the satellite over pass (Liang et al., 2002). Therefore, downscaling of hybrid method seems necessary. The Landsat and the Advanced Space-borne Thermal Emission Reflectance Radiometer (ASTER) provide the spatial resolution less than 100 m, but routine application is hindered by the low frequency of repeated coverage (~ 16 days). If satellite data at finer spatial resolution were available, the first step to apply hybrid method is to obtain Top-Of-Atmosphere (TOA) reflectance and surface radiation corresponding to finer satellite data using radiative transfer simulation. This leads to the step for establishing relationship between them, estimation can be easily implemented once the relationship is established. However, it should be noted that selected channels in simulation have enough information to influence SRB such as aerosols, clouds, water vapors and other gases. There is no computational or technical limitation to apply hybrid method to finer sensor data than 1 km, however, consideration on space and time mismatch and atmospheric heterogeneity issue should be seriously taken. Optical depth variability and the horizontal transport effect of light moving between cloud columns (usually referred to as 3-D cloud effect) affects the accurate estimation of SRB. As shown in section 2.4.3, aggregation to 9 km resolution mitigates 3-D cloud effect.

5.4 Future research issues

The new hybrid method developed in this study is validated at seven operating SURFRAD sites. These sites represent various land cover types in the United States; however, an evaluation process on other land cover types, at a greater range of geographical location, and at various elevations is necessary. The new hybrid method is easily implemented to generate regional and global products at a finer resolution and the scheme is applicable to other sensors like Geostationary Operational Environmental Satellites (GOES).

In addition to the expanded evaluation of the hybrid method of estimating S_n , more validation in cloudy-sky R_n is also recommended. Then cloudy-sky R_n can be combined to the estimated clear-sky L_n from satellite data to produce all-sky R_n at finer resolution, which will be valuable in numerical weather and land surface models. The finer resolution data can be used to validate coarser resolution datasets.

Daily integrated S_n has comparable accuracy with the existing method, however, it overcomes limits in spatial coverage of the existing method. An increase in the number of instantaneous estimations of S_n will increase the accuracy of the adjusted sinusoidal interpolation; therefore, use of geostationary satellite data with more observations per day is suggested.

Diagnosing surface radiation budget that constitute the land surface water and energy budget is important and Surface Radiation Budget (SRB) product at high spatial resolution is necessary specifically in land applications because current products have fine temporal resolution and coarse spatial resolution. The ability to obtain accurate estimates of large-scale geophysical variables from remote sensing observations is especially important since the ground-based data needed for forward

modeling is sparse in many regions of the globe. Heterogeneity in many surface and surface processes often require that models be applied at relatively high spatial and temporal resolution. Also research questions focusing on change detection and variability as well as validation require high spatial resolution and spatial resolution of the product developed in this study may not be fine enough. One of approaches to obtain surface radiation at finer spatial resolution is to use data assimilation method to downscale the coarser product. It can be done by combining all available information essentially consisting of observations and physical laws which govern the evolution of the system. The selection of a data assimilation procedure appropriate for a given application is a balance between making the best use of available information, computational efficiency, flexibility, and robustness (Reichle et al., 2002). Recent applications have shown that the Ensemble Kalman Filter (EnKF) is an attractive option for land surface data assimilation based on its modular structure and flexibility in comparison to other techniques (Margulis and Entekhabi, 2003; Margulis and Entekhabi, 2004).

Finer spatial resolution SRB product with improved accuracy will be able to support to estimate Net Primary Production (NPP)/ Gross Primary Production (GPP) and to capture variability of surface energy flux such as evapotranspiration. Assumptions concerning the source and magnitude of error should be considered carefully when data assimilation and use of assimilated data to land surface model. Because inappropriate model error assumptions can lead to circumstances in which assimilated observation actually degrades the performance of land surface model (Crow and Van Loon, 2006). Numerical investigation of SRB impact in those land

surface and climate model should be followed and this will help to understand the sensitivity of land surface and the earth's climate, further, to predict their change.

Acronyms

ANN – artificial neural network
CAVE – CERES/ARM validation Experiment
CEOS – Committee on Earth Observation Satellites
CERES – Clouds and the Earth’s Radiant Energy System
CRS – Clouds and Radiation Swath
ECWMF – European Centre for Medium-Range Weather Forecasts
EOS – Earth Observing System
ERBE – Earth Radiation Budget Experiment
EVI – enhanced vegetation index
GCIP/GAPP – GEWEX Continental scale International Project and GEWEX Americas Prediction Project
GCOS – Global Climate Observation System
GEWEX – Global Energy and Water Cycle Experiments
GOES – Geostationary Operational Environmental Satellites
ISCCP – International Satellite Cloud Climatology project
 L_n – surface longwave net radiation
MISR – Multi-angle Imaging SpectroRadiometer
MODIS – Moderate Resolution Imaging Spectroradiometer
MODTRAN4 – Moderate Resolution Transmittance Code Version 4
MCST – MODIS Characterization and Support Team
NASA – National Aeronautics and Space Administration (NASA)
NCAR – National Center for Atmospheric Research
NCEP – National Centers for Environmental Prediction
NESDIS – National Environmental Satellite Data and Information Service
NOAA – National Oceanic and Atmospheric Administration
PFT – plant functional type
RMSE – root mean squared error
 R_n – surface all-wave net radiation
 S_{\downarrow} – surface shortwave downward radiation
 S_{\uparrow} – surface shortwave upward radiation
 S_n – surface Shortwave Net Radiation
SRB – surface radiation budget
SURFRAD – Surface Radiation Budget Network
TIROS – Television and InfraRed Observation Satellite
TOA – top of atmosphere
TOVS – TIROS Operational Vertical Sounder
TRMM – Tropical Rainfall Measuring Mission
WCRP – World Climate Research Programme
WMO – World Meteorological Organization

Bibliography

- Alados, I., Foyo-Moreno, I., Olmo, F.J. and Alados-Arboledas, L., 2003, Relationship between net radiation and solar radiation for semi-arid shrub-land. *Agricultural and Forest Meteorology*, **116(3-4)**: 221-227.
- Alexandrov, V.A. and Hoogenboom, G., 2000, The impact of climate variability and change on crop yield in Bulgaria. *Agricultural and Forest Meteorology*, **104(4)**: 315-327.
- Allen, R.G., 1996, Assessing integrity of weather data for reference evapotranspiration estimation. *Journal of Irrigation and Drainage Engineering-Asce*, **122(2)**: 97-106.
- Annear, R.L. and Wells, S.A., 2007, A comparison of five models for estimating clear-sky solar radiation. *Water Resources Research*, **43(10)**.
- Augustine, J.A., Hodges, G.B., Cornwall, C.R., Michalsky, J.J. and Medina, C.I., 2005, An update on SURFRAD - The GCOS Surface Radiation budget network for the continental United States. *Journal of Atmospheric and Oceanic Technology*, **22(10)**: 1460-1472.
- Baldocchi, D., Falge, E., Gu, L.H., Olson, R., Hollinger, D., Running, S., Anthoni, P., Bernhofer, C., Davis, K., Evans, R., Fuentes, J., Goldstein, A., Katul, G., Law, B., Lee, X.H., Malhi, Y., Meyers, T., Munger, W., Oechel, W., U, K.T.P., Pilegaard, K., Schmid, H.P., Valentini, R., Verma, S., Vesala, T., Wilson, K. and Wofsy, S., 2001, FLUXNET: A new tool to study the temporal and spatial variability of ecosystem-scale carbon dioxide, water vapor, and energy flux densities. *Bulletin of the American Meteorological Society*, **82(11)**: 2415-2434.
- Barker, H.W. and Davies, J.A., 1992, Cumulus Cloud Radiative Properties and the Characteristics of Satellite Radiance Wave-Number Spectra. *Remote Sensing of Environment*, **42(1)**: 51-64.
- Berk, A., Anderson, G.P., Acharya, P.K., Chetwynd, J.H., Bernstein, L.S., Shettle, E.P., Matthew, M.W. and Adler-Golden, S.M., 1999. MODTRAN4 user's manual, AIR FORCE RESEARCH LABORATORY, Space Vehicles Directorate, and AIR FORCE MATERIEL COMMAND, HANSCOM AFB, MA.
- Berk, A., Anderson, G.P., Acharya, P.K., Hoke, M.L., Chetwynd, J.H., Bernstein, L.S., Shettle, E.P., Matthew, M.W. and Adler-Golden, S.M., 2003, MODTRAN4 Version3 Revision1 User's Manual.
- Bromwich, D.H., Bai, L.H. and Bjarnason, G.G., 2005, High-resolution regional climate simulations over Iceland using Polar MM5. *Monthly Weather Review*, **133(12)**: 3527-3547.
- Cahalan, R.F., Ridgway, W., Wiscombe, W.J., Gollmer, S. and Harshvardhan, 1994, Independent Pixel and Monte-Carlo Estimates of Stratocumulus Albedo. *Journal of the Atmospheric Sciences*, **51(24)**: 3776-3790.

- Cano, D., Monget, J.M., Albuissou, M., Guillard, H., Regas, N. and Wald, L., 1986, A Method for the Determination of the Global Solar-Radiation from Meteorological Satellite Data. *Solar Energy*, **37(1)**: 31-39.
- CEOS and WMO, 2000, <http://192.91.247.60/sat/aspscripts/Requirements.asp>.
- Cess, R.D., Dutton, E.G., Deluisi, J.J. and Jiang, F., 1991, Determining Surface Solar Absorption from Broad-Band Satellite Measurements for Clear Skies - Comparison with Surface Measurements. *Journal of Climate*, **4(2)**: 236-247.
- Cess, R.D. and Vulis, I.L., 1989, Inferring Surface Solar Absorption from Broadband Satellite Measurements *Journal of Climate*, **2(9)**: 974-985.
- Cess, R.D., Zhang, M.H., Minnis, P., Corsetti, L., Dutton, E.G., Forgan, B.W., Garber, D.P., Gates, W.L., Hack, J.J., Harrison, E.F., Jing, X., Kiehl, J.T., Long, C.N., Morcrette, J.J., Potter, G.L., Ramanathan, V., Subasilar, B., Whitlock, C.H., Young, D.F. and Zhou, Y., 1995, Absorption of Solar-Radiation by Clouds - Observations Versus Models. *Science*, **267(5197)**: 496-499.
- Chen, B.Z., Chen, J.M. and Ju, W.M., 2007, Remote sensing-based ecosystem-atmosphere simulation scheme (EASS) - Model formulation and test with multiple-year data. *Ecological Modelling*, **209(2-4)**: 277-300.
- Chen, Y.M., Liang, S., Wang, J., Kim, H.Y. and Martonchik, J.V., 2008, Validation of the MISR land surface broadband albedo. *International journal of remote sensing*: submitted.
- Collins, W.D., Bitz, C.M., Blackmon, M.L., Bonan, G.B., Bretherton, C.S., Carton, J.A., Chang, P., Doney, S.C., Hack, J.J., Henderson, T.B., Kiehl, J.T., Large, W.G., McKenna, D.S., Santer, B.D. and Smith, R.D., 2006, The Community Climate System Model version 3 (CCSM3). *Journal of Climate*, **19(11)**: 2122-2143.
- Crow, W.T. and Van Loon, E., 2006, Impact of incorrect model error assumptions on the sequential assimilation of remotely sensed surface soil moisture. *Journal of Hydrometeorology*, **7(3)**: 421-432.
- De Haan, L.L. and Kanamitsu, M., 2007, A comparison of the Noah and OSU land surface models in the ECPC seasonal forecast model. *Journal of Hydrometeorology*, **8(5)**: 1031-1048.
- Dedieu, G., Deschamps, P.Y. and Kerr, Y.H., 1987, Satellite Estimation of Solar Irradiance at the Surface of the Earth and of Surface Albedo Using a Physical Model Applied to Meteosat Data. *Journal of Climate and Applied Meteorology*, **26(1)**: 79-87.
- Diak, G.R. and Gautier, C., 1983, Improvements to a Simple Physical Model for Estimating Insolation from Goes Data. *Journal of Climate and Applied Meteorology*, **22(3)**: 505-508.
- Ellingson, R.G., 1995, Surface Longwave Fluxes from Satellite-Observations - a Critical-Review. *Remote Sensing of Environment*, **51(1)**: 89-97.
- Fang, H.L., Liang, S., Kim, H.-Y., Townshend, J.R., Schaaf, C., Strahler, A. and Dickinson, R., 2007, Developing a spatially continuous 1 km surface albedo data set over North America from Terra MODIS products. *Journal of Geophysical Research-Atmospheres*, **112**: doi:10.1029/2006JD008377.

- Fletcher, A.L. and Moot, D.J., 2007, Estimating daily solar radiation in New Zealand using air temperatures. *New Zealand Journal of Crop and Horticultural Science*, **35(1)**: 147-157.
- Forster, P.M.D. and Gregory, J.M., 2006, The climate sensitivity and its components diagnosed from Earth Radiation Budget data. *Journal of Climate*, **19(1)**: 39-52.
- Fritschen, L.J. and Ping, Q., 1992, Variation in Energy-Balance Components from 6 Sites in a Native Prairie for 3 Years. *Journal of Geophysical Research-Atmospheres*, **97(D17)**: 18651-18661.
- Frouin, R. and Chertock, B., 1992, A Technique for Global Monitoring of Net Solar Irradiance at the Ocean Surface .1. Model. *Journal of Applied Meteorology*, **31(9)**: 1056-1066.
- Garatuza-Payan, J., Pinker, R.T., Shuttleworth, W.J. and Watts, C.J., 2001, Solar radiation and evapotranspiration in northern Mexico estimated from remotely sensed measurements of cloudiness. *Hydrological Sciences Journal-Journal Des Sciences Hydrologiques*, **46(3)**: 465-478.
- Gautier, C., Diak, G. and Masse, S., 1980, A Simple Physical Model to Estimate Incident Solar-Radiation at the Surface from Goes Satellite Data. *Journal of Applied Meteorology*, **19(8)**: 1005-1012.
- GCOS, 2006. Systematic observation requirements for satellite-based products for climate.
- Goward, S.N., Davis, P.E., Fleming, D., Miller, L. and Townshend, J.R., 2003, Empirical comparison of Landsat 7 and IKONOS multispectral measurements for selected Earth Observation System (EOS) validation sites. *Remote Sensing of Environment*, **88(1-2)**: 80-99.
- Guan, H., Tremblay, A., Isaac, G.A. and Strawbridge, K.B., 2000, Numerical simulations of stratus clouds and their sensitivity to radiation - A RACE case study. *Journal of Applied Meteorology*, **39(11)**: 1881-1893.
- Hansen, S., 2000, *Markvandsbalance, Appendix A: Estimation of net radiation. Technical note*. The Royal Veterinary and Agricultural University, Copenhagen, 28 pp.
- Hay, J.E. and Hanson, K.J., 1978, Satellite-Based Methodology for Determining Solar Irradiance at the Ocean Surface During Gate. *Bulletin of the American Meteorological Society*, **59(11)**: 1549-1549.
- Holben, B.N. and Eck, T.F., 1990, Precipitable Water in the Sahel Measured Using Sun Photometry. *Agricultural and Forest Meteorology*, **52(1-2)**: 95-107.
- Hunt, E.R., Martin, F.C. and Running, S.W., 1991, Simulating the Effects of Climatic Variation on Stem Carbon Accumulation of a Ponderosa Pine Stand - Comparison with Annual Growth Increment Data. *Tree Physiology*, **9(1-2)**: 161-171.
- Hunt, L.A., Kuchar, L. and Swanton, C.J., 1998, Estimation of solar radiation for use in crop modelling. *Agricultural and Forest Meteorology*, **91(3-4)**: 293-300.
- Irmak, S., Irmak, A., Jones, J.W., Howell, T.A., Jacobs, J.M., Allen, R.G. and Hoogenboom, G., 2003a, Predicting daily net radiation using minimum climatological data. *Journal of Irrigation and Drainage Engineering-Asce*, **129(4)**: 256-269.

- Jacobs, J.M., Anderson, M.C., Friess, L.C. and Diak, G.R., 2004, Solar radiation, longwave radiation and emergent wetland evapotranspiration estimates from satellite data in Florida, USA. *Hydrological Sciences Journal-Journal Des Sciences Hydrologiques*, **49(3)**: 461-476.
- Jacobs, J.M., Myers, D.A., Anderson, M.C. and Diak, G.R., 2002, GOES surface insolation to estimate wetlands evapotranspiration. *Journal of Hydrology*, **266(1-2)**: 53-65.
- Justice, C., Belward, A., Morisette, J., Lewis, P., Privette, J. and Baret, F., 2000, Developments in the 'validation' of satellite sensor products for the study of the land surface. *International Journal of Remote Sensing*, **21(17)**: 3383-3390.
- Kaminsky, K.Z. and Dubayah, R., 1997, Estimation of surface net radiation in the boreal forest and northern prairie from shortwave flux measurements. *Journal of Geophysical Research-Atmospheres*, **102(D24)**: 29707-29716.
- Kim, H.Y., Liang, S. and Fang, H., 2008, Mapping the UV surface albedo from MODIS albedo products. *International journal of remote sensing*: in 2nd revision.
- Kjaersgaard, J.H., Cuenca, R.H., Plauborg, F.L. and Hansen, S., 2007, Long-term comparisons of net radiation calculation schemes. *Boundary-Layer Meteorology*, **123(3)**: 417-431.
- Kustas, W.P., Li, F., Jackson, T.J., Prueger, J.H., MacPherson, J.I. and Wolde, M., 2004, Effects of remote sensing pixel resolution on modeled energy flux variability of croplands in Iowa. *Remote Sensing of Environment*, **92(4)**: 535-547.
- Kustas, W.P. and Norman, J.M., 2000, Evaluating the effects of subpixel heterogeneity on pixel average fluxes. *Remote Sensing of Environment*, **74(3)**: 327-342.
- Kustas, W.P., Norman, J.M., Anderson, M.C. and French, A.N., 2003, Estimating subpixel surface temperatures and energy fluxes from the vegetation index-radiometric temperature relationship. *Remote Sensing of Environment*, **85(4)**: 429-440.
- Li, F.Q., Kustas, W.P., Anderson, M.C., Prueger, J.H. and Scott, R.L., 2008, Effect of remote sensing spatial resolution on interpreting tower-based flux observations. *Remote Sensing of Environment*, **112(2)**: 337-349.
- Li, Z.Q., Leighton, H.G. and Cess, R.D., 1993b, Surface Net Solar-Radiation Estimated from Satellite Measurements - Comparisons with Tower Observations. *Journal of Climate*, **6(9)**: 1764-1772.
- Li, Z.Q., Leighton, H.G., Masuda, K. and Takashima, T., 1993a, Estimation of Sw Flux Absorbed at the Surface from Toa Reflected Flux. *Journal of Climate*, **6(2)**: 317-330.
- Li, Z.Q. and Trishchenko, A.P., 2001, Quantifying uncertainties in determining SW cloud radiative forcing and cloud absorption due to variability in atmospheric conditions. *Journal of the Atmospheric Sciences*, **58(4)**: 376-389.
- Liang, S., 2004, *Quantitative Remote Sensing of Land Surfaces*. John Wiley and sons, Inc., Hoboken, N.J., 534 pp.
- Liang, S.L., Fang, H.L., Chen, M.Z., Shuey, C.J., Walthall, C., Daughtry, C., Morisette, J., Schaaf, C. and Strahler, A., 2002, Validating MODIS land

- surface reflectance and albedo products: methods and preliminary results. *Remote Sensing of Environment*, **83(1-2)**: 149-162.
- Loeb, N.G., Varnai, T. and Winker, D.M., 1998, Influence of subpixel-scale cloud-top structure on reflectances from overcast stratiform cloud layers. *Journal of the Atmospheric Sciences*, **55(18)**: 2960-2973.
- Ma, Y.M., Su, Z.B., Li, Z.L., Koike, T. and Menenti, M., 2002, Determination of regional net radiation and soil heat flux over a heterogeneous landscape of the Tibetan Plateau. *Hydrological Processes*, **16(15)**: 2963-2971.
- Margulis, S.A. and Entekhabi, D., 2003, Variational assimilation of radiometric surface temperature and reference-level micrometeorology into a model of the atmospheric boundary layer and land surface. *Monthly Weather Review*, **131(7)**: 1272-1288.
- Margulis, S.A. and Entekhabi, D., 2004, Boundary-layer entrainment estimation through assimilation of radiosonde and micrometeorological data into a mixed-layer model. *Boundary-Layer Meteorology*, **110(3)**: 405-433.
- Masson, V., Champeaux, J.L., Chauvin, F., Meriguet, C. and Lacaze, R., 2003, A global database of land surface parameters at 1-km resolution in meteorological and climate models. *Journal of Climate*, **16(9)**: 1261-1282.
- Masuda, K., Leighton, H.G. and Li, Z.Q., 1995, A New Parameterization for the Determination of Solar Flux Absorbed at the Surface from Satellite Measurements. *Journal of Climate*, **8(6)**: 1615-1629.
- Moran, M.S., Humes, K.S. and Pinter, P.J., 1997, The scaling characteristics of remotely-sensed variables for sparsely-vegetated heterogeneous landscapes. *Journal of Hydrology*, **190(3-4)**: 337-362.
- Nishida, K., Nemani, R.R., Running, S.W. and Glassy, J.M., 2003a, An operational remote sensing algorithm of land surface evaporation. *Journal of Geophysical Research-Atmospheres*, **108(D9)**.
- Noble, P.A. and Tribou, E.H., 2007, Neuroet: An easy-to-use artificial neural network for ecological and biological modeling. *Ecological Modelling*, **203(1-2)**: 87-98.
- Noia, M., Ratto, C.F. and Festa, R., 1993, Solar Irradiance Estimation from Geostationary Satellite Data .2. Physical Models. *Solar Energy*, **51(6)**: 457-465.
- Perez, R., Ineichen, P., Moore, K., Kmiecik, M., Chain, C., George, R. and Vignola, F., 2002, A new operational model for satellite-derived irradiances: Description and validation. *Solar Energy*, **73(5)**: 307-317.
- Pinker, R.T., Ewing, J.A. and Tarpley, J.D., 1985, The Relationship between the Planetary and Surface Net-Radiation. *Journal of Climate and Applied Meteorology*, **24(11)**: 1262-1268.
- Pinker, R.T., Frouin, R. and Li, Z., 1995, A Review of Satellite Methods to Derive Surface Shortwave Irradiance. *Remote Sensing of Environment*, **51(1)**: 108-124.
- Pinker, R.T. and Laszlo, I., 1990, Improved Prospects for Estimating Insolation for Calculating Regional Evapotranspiration from Remotely Sensed Data. *Agricultural and Forest Meteorology*, **52(1-2)**: 227-251.

- Pinker, R.T. and Laszlo, I., 1992, Modeling Surface Solar Irradiance for Satellite Applications on a Global Scale. *Journal of Applied Meteorology*, **31(2)**: 194-211.
- Pinker, R.T., Li, X., Meng, W. and Yegorova, E.A., 2007, Toward improved satellite estimates of short-wave radiative fluxes - Focus on cloud detection over snow: 2. Results. *Journal of Geophysical Research-Atmospheres*, **112(D9)**.
- Pinker, R.T., Tarpley, J.D., Laszlo, I., Mitchell, K.E., Houser, P.R., Wood, E.F., Schaake, J.C., Robock, A., Lohmann, D., Cosgrove, B.A., Sheffield, J., Duan, Q.Y., Luo, L.F. and Higgins, R.W., 2003, Surface radiation budgets in support of the GEWEX Continental-Scale International Project (GCIP) and the GEWEX Americas Prediction Project (GAPP), including the North American Land Data Assimilation System (NLDAS) Project. *Journal of Geophysical Research-Atmospheres*, **108(D22)**.
- Reichle, R.H., McLaughlin, D.B. and Entekhabi, D., 2002, Hydrologic data assimilation with the ensemble Kalman filter. *Monthly Weather Review*, **130(1)**: 103-114.
- Rivington, M., Bellocchi, G., Matthews, K.B. and Buchan, K., 2005, Evaluation of three model estimations of solar radiation at 24 UK stations. *Agricultural and Forest Meteorology*, **132(3-4)**: 228-243.
- Roesch, A. and Roeckner, E., 2006, Assessment of snow cover and surface albedo in the ECHAM5 general circulation model. *Journal of Climate*, **19(16)**: 3828-3843.
- Rossow, W.B. and Schiffer, R.A., 1991, Isccp Cloud Data Products. *Bulletin of the American Meteorological Society*, **72(1)**: 2-20.
- Rossow, W.B. and Zhang, Y.C., 1995, Calculation of Surface and Top of Atmosphere Radiative Fluxes from Physical Quantities Based on Isccp Data Sets .2. Validation and First Results. *Journal of Geophysical Research-Atmospheres*, **100(D1)**: 1167-1197.
- Salomon, J.G., Schaaf, C.B., Strahler, A.H., Gao, F. and Jin, Y.F., 2006, Validation of the MODIS Bidirectional Reflectance Distribution Function and Albedo retrievals using combined observations from the Aqua and Terra platforms. *Ieee Transactions on Geoscience and Remote Sensing*, **44(6)**: 1555-1565.
- Samani, Z., Bawazir, A.S., Bleiweiss, M., Skaggs, R. and Tran, V.D., 2007, Estimating daily net radiation over vegetation canopy through remote sensing and climatic data. *Journal of Irrigation and Drainage Engineering-Asce*, **133(4)**: 291-297.
- Schaaf, C.B., Gao, F., Strahler, A.H., Lucht, W., Li, X.W., Tsang, T., Strugnell, N.C., Zhang, X.Y., Jin, Y.F., Muller, J.P., Lewis, P., Barnsley, M., Hobson, P., Disney, M., Roberts, G., Dunderdale, M., Doll, C., d'Entremont, R.P., Hu, B.X., Liang, S.L., Privette, J.L. and Roy, D., 2002, First operational BRDF, albedo nadir reflectance products from MODIS. *Remote Sensing of Environment*, **83(1-2)**: 135-148.
- Schmetz, J., 1989, Towards a surface radiation climatology: Retrieval of downward irradiance from satellites. *Atmospheric Research*, **23**: 237 - 321.

- Soci, C., Fischer, C. and Horanyi, A., 2006, Sensitivity of high-resolution forecasts using the adjoint technique at the 10-km scale. *Monthly Weather Review*, **134(3)**: 772-790.
- Stackhouse, P., 2004, 12-year Surface Radiation Budget Data Set. *GEWEX News*, **14**: 10-10.
- Stewart, J.B., Watts, C.J., Rodriguez, J.C., De Bruin, H.A.R., van den Berg, A.R. and Garatuza-Payan, J., 1999, Use of satellite data to estimate radiation and evaporation for northwest Mexico. *Agricultural Water Management*, **38(3)**: 181-193.
- Tang, B.H., Li, Z.L. and Zhang, R.H., 2006, A direct method for estimating net surface shortwave radiation from MODIS data. *Remote Sensing of Environment*, **103(1)**: 115-126.
- Tarpley, J.D., 1979, Estimating Incident Solar-Radiation at the Surface from Geostationary Satellite Data. *Journal of Applied Meteorology*, **18(9)**: 1172-1181.
- Tian, Y.H., Woodcock, C.E., Wang, Y.J., Privette, J.L., Shabanov, N.V., Zhou, L.M., Zhang, Y., Buermann, W., Dong, J.R., Veikkanen, B., Hame, T., Andersson, K., Ozdogan, M., Knyazikhin, Y. and Myneni, R.B., 2002, Multiscale analysis and validation of the MODIS LAI product - I. Uncertainty assessment. *Remote Sensing of Environment*, **83(3)**: 414-430.
- Toller, G.N., Isaacman, A., Kuyper, J. and Salomonson, V., 2006, MODIS Level 1B Product User's Guide. *NASA/Goddard Space Flight Center*.
- Townshend, J.R.G. and Justice, C.O., 1988, Selecting the Spatial-Resolution of Satellite Sensors Required for Global Monitoring of Land Transformations. *International Journal of Remote Sensing*, **9(2)**: 187-236.
- Treitz, P. and Howarth, P., 2000, High spatial resolution remote sensing data for forest ecosystem classification: An examination of spatial scale. *Remote Sensing of Environment*, **72(3)**: 268-289.
- Trnka, M., Eitzinger, J., Kapler, P., Dubrovsky, M., Semerádova, D., Zalud, Z. and Formayer, H., 2007, Effect of estimated daily global solar radiation data on the results of crop growth models. *Sensors*, **7(10)**: 2330-2362.
- Varnai, T., 2000, Influence of three-dimensional radiative effects on the spatial distribution of shortwave cloud reflection. *Journal of the Atmospheric Sciences*, **57(2)**: 216-229.
- Wang, D., Liang, S. and Zheng, T., 2008a, Estimation of Daily-integrated PAR from MODIS Data. *International Journal of Remote Sensing*: in revision.
- Wang, K.C., 2008, Water vapor effect in solar radiation estimation. to be submitted.
- Wang, K.C., Liang, S., Wang, D. and Zheng, T., 2008b, Simultaneous estimation of surface photosynthetically active radiation and albedo from GOES. *Remote Sensing of Environment*: in revision.
- Wang, K.C., Liu, J.M., Zhou, X.J., Sparrow, M., Ma, M., Sun, Z. and Jiang, W.H., 2004a, Validation of the MODIS global land surface albedo product using ground measurements in a semidesert region on the Tibetan Plateau. *Journal of Geophysical Research-Atmospheres*, **109(D5)**.

- Wang, W. and Liang, S., 2008, Estimating High Spatial Resolution Clear-sky Land Surface Longwave Radiation Budget from MODIS and GOES Data. *International Geoscience and Remote Sensing Symposium*: in revision.
- Wang, Z., Zeng, X., Barlage, M., Dickinson, R.E., Gao, F. and Schaaf, C.B., 2004b, Using MODIS BRDF and albedo data to evaluate global model land surface albedo. *Journal of Hydrometeorology*, **5(1)**: 3-14.
- Whitlock, C.H., Charlock, T.P., Staylor, W.F., Pinker, R.T., Laszlo, I., Ohmura, A., Gilgen, H., Konzelman, T., Dipasquale, R.C., Moats, C.D., Lecroy, S.R. and Ritchey, N.A., 1995, First Global Wcrp Shortwave Surface Radiation Budget Dataset. *Bulletin of the American Meteorological Society*, **76(6)**: 905-922.
- Wielicki, B.A., Barkstrom, B.R., Baum, B.A., Charlock, T.P., Green, R.N., Kratz, D.P., Lee, R.B., Minnis, P., Smith, G.L., Wong, T.M., Young, D.F., Cess, R.D., Coakley, J.A., Crommelynck, D.A.H., Donner, L., Kandel, R., King, M.D., Miller, A.J., Ramanathan, V., Randall, D.A., Stowe, L.L. and Welch, R.M., 1998, Clouds and the Earth's Radiant Energy System (CERES): Algorithm overview. *IEEE Transactions on Geoscience and Remote Sensing*, **36(4)**: 1127-1141.
- Wolf, J., Evans, L.G., Semenov, M.A., Eckersten, H. and Iglesias, A., 1996, Comparison of wheat simulation models under climate change .1. Model calibration and sensitivity analyses. *Climate Research*, **7(3)**: 253-270.
- Wu, G.F., Liu, Y.L. and Wang, T.J., 2007, Methods and strategy for modeling daily global solar radiation with measured meteorological data - A case study in Nanchang station, China. *Energy Conversion and Management*, **48(9)**: 2447-2452.
- Xia, X.A., Wang, P.C., Chen, H.B. and Liang, F., 2006, Analysis of downwelling surface solar radiation in China from National Centers for Environmental Prediction reanalysis, satellite estimates, and surface observations. *Journal of Geophysical Research-Atmospheres*, **111(D9)**.
- Zhang, G.P., 2007, Avoiding pitfalls in neural network research. *Ieee Transactions on Systems Man and Cybernetics Part C-Applications and Reviews*, **37(1)**: 3-16.
- Zhang, Y.C., Rossow, W.B. and Lacis, A.A., 1995, Calculation of Surface and Top of Atmosphere Radiative Fluxes from Physical Quantities Based on Isccp Data Sets .1. Method and Sensitivity to Input Data Uncertainties. *Journal of Geophysical Research-Atmospheres*, **100(D1)**: 1149-1165.
- Zhang, Y.C., Rossow, W.B., Lacis, A.A., Oinas, V. and Mishchenko, M.I., 2004, Calculation of radiative fluxes from the surface to top of atmosphere based on ISCCP and other global data sets: Refinements of the radiative transfer model and the input data. *Journal of Geophysical Research-Atmospheres*, **109(D19)**.
- Zhao, M., Running, S.W. and Nemani, R.R., 2006, Sensitivity of Moderate Resolution Imaging Spectroradiometer (MODIS) terrestrial primary production to the accuracy of meteorological reanalyses. *Journal of Geophysical Research-Biogeosciences*, **111(G1)**.
- Zhou, L., Dickinson, R.E., Tian, Y., Zeng, X., Dai, Y., Yang, Z.L., Schaaf, C.B., Gao, F., Jin, Y., Strahler, A., Myneni, R.B., Yu, H., Wu, W. and Shaikh, M., 2003, Comparison of seasonal and spatial variations of albedos from Moderate-

Resolution Imaging Spectroradiometer (MODIS) and Common Land Model.
Journal of Geophysical Research-Atmospheres, **108(D15)**.